DEVELOPMENT OF ELECTROCHEMICAL MICRO MACHINING

A Thesis

by

SRIHARSHA SRINIVAS SUNDARRAM

Submitted to the Office of Graduate Studies of
Texas A&M University
in partial fulfillment of the requirements for the degree of

MASTER OF SCIENCE

August 2008

Major Subject: Mechanical Engineering

DEVELOPMENT OF ELECTROCHEMICAL MICRO MACHINING

A Thesis

by

SRIHARSHA SRINIVAS SUNDARRAM

Submitted to the Office of Graduate Studies of
Texas A&M University
in partial fulfillment of the requirements for the degree of

MASTER OF SCIENCE

Approved by:

Chair of Committee,	Nguyen P. Hung
Committee Members,	Terry Creasy
	Jyhwen Wang
Head of Department,	Dennis L. O'Neal

August 2008

Major Subject: Mechanical Engineering

ABSTRACT

Development of Electrochemical Micro Machining. (August 2008)

Sriharsha Srinivas Sundarram, B.E., Anna University, India

Chair of Advisory Committee: Dr. Nguyen P. Hung

The machining of materials on micrometer and sub-micrometer scale is considered the technology of the future. The current techniques for micro manufacturing mostly are silicon based. These manufacturing techniques are not suitable for use in demanding applications like aerospace and biomedical industries. Micro electrochemical machining (μECM) removes material while holding micron tolerances and μECM can machine hard metals and alloys.

This study aims at developing a novel μECM utilizing high frequency voltage pulses and closed loop control. Stainless steel SS-316L and copper alloy CA-173 were chosen as the workpiece materials. A model was developed for material removal rate.

The research studied the effect of various parameters such as voltage, frequency, pulse ON/OFF time, and delay between pulses of the stepper motor on the machined profiles. Experimental data on small drilled holes agreed with theoretical models within 10%. Micro burrs can be effectively removed by optimal μECM. A sacrificial layer helped to improve the hole profile since it reduced 43% of corner rounding.

ACKNOWLEDGEMENTS

This material is based upon work supported by the National Science Foundation under grant No. 0552885. I would like to thank my committee chair, Dr. Hung, and my committee members, Dr. Creasy and Dr. Wang, for their guidance and support throughout the course of this research.

I would like to thank my colleague, Ozkeskin, in Micro/nano manufacturing lab for helping me throughout the work. Thanks also go to my friends and the department faculty and staff for making my time at Texas A&M University a great experience.

I would like to thank our sponsor, Agilent Technologies, and collaborators, Galnik, Mexico and Cideteq, Mexico, for their generous support without which the project would not have materialized.

Finally, thanks to my mother and father for their encouragement and to my uncle Gopal and aunt Padmaja for their support.

TABLE OF CONTENTS

Page

Page

LIST OF FIGURES

FIGURE Page

FIGURE Page

FIGURE Page

LIST OF TABLES

LIST OF SYMBOLS

A = Surface area of tool

A_w = Molecular mass

b = Number of burrs under tool

C = Electrochemical constant

C_{sat} = Surface concentration

D = Effective diffusion coefficient

E = Voltage

f = Feed rate

F = Faraday's constant

g = Gap between the tool and the workpiece

h = Height of burrs

i_l = Anodic limiting current density

I = Current

K = Conductivity

K_V = Electrochemical machinability coefficient

l = Length of edge of workpiece

L = Characteristic length

M = Molecular weight of dissolved material

n = Apparent dissolution valence

N = Number of pulses

P = Period of sine curve

r = Resistivity of the electrolyte

R = Resistance

S = Speed of electrode

Sh = Sherwood number

t = Time

U = Working voltage

V = Volume of metal removed

V_s = Volume of single burr

V_l = Volume of burrs along length l

V_u = Unit volume removed

V_f = Feed rate of electrode

ΔV = Over voltage

ΔW = Anodic weight loss

Y_e = Equilibrium gap

Z = Number of valence electrons

Z'= Reading of laser sensor

ρ = Density of work material

δ = Diffusion-layer thickness

τ = Pulse duration

1. INTRODUCTION

Material removal techniques have a pivotal role to play in component fabrication. In recent years many high strength alloys such as copper beryllium and titanium alloys were produced that are extremely difficult to machine using the traditional processes. These alloys were developed for a variety of industries ranging from aerospace to medical engineering. Machining these alloys with conventional tools results in subsurface damage of the workpiece and in tool

damage. The tool size and geometry

limit the final component shape that can be machined. Another problem with these tools is that they tend to leave burrs on the machined surface. These burrs are undesirable in many applications. For example, in the medical industry the presence of even very small burrs will damage living tissues where these machined parts are used as implants. In electronic devices where a number of components are in close contact, the burrs may lead to short circuits. In mechanical components burrs may result in a misfit. Electrochemical machining (ECM) can machine these alloys. Devices are becoming smaller as time progresses but their features are increasing at the same time. Machining materials on micro and sub-micro scale is considered a key technology for miniaturizing mechanical parts and complete machines.

Micro manufacturing techniques find application in various industries such as electro-communications, semi-conductors, medicine, and ultra-precision machinery. A

This thesis follows the style of *Journal of Manufacturing Systems*.

suitable manufacturing technique for mass production of these micro scale components needs to be established. The current techniques used for machining these components are mainly the dry vacuum process and wet chemical etching (Datta 1998).

These techniques come under the non-conventional machining processes category. The major difference between conventional and non-conventional machining processes is that conventional processes use a sharp tool for material removal by physical means where as the non-conventional techniques remove material by utilizing chemical, thermal, or electrical energy or a combination of these energies (Groover 2006). These processes suffer from several inherent problems. Dry-etching techniques require high cost equipment and do not offer good selectivity in material removal. The chemicals used in wet etching processes are commonly toxic and extreme care has to be taken to dispose of them.

These techniques can precisely perform 2D machining at the micro level, that is, they can machine thin films extremely well. However, they are unable to produce 3D components and components with high aspect ratio.

Most of these techniques were developed for the electronics industry specifically silicon. Silicon does not find applications in fields other than the electronics industry because it is toxic. High exposure to silicon dust causes chronic respiratory problems (Lenntech 1998). These techniques also suffer from limitations such as restricted materials choice, inability to produce complex profiles, and huge investment for facilities and equipment (Rajurkar et al. 2006).

Electrochemical machining is a non-conventional process that found wide-spread

applications because offered these advantages:

1. It can machine difficult to cut materials, generate complex contours, produce a stress free surface, and have no tool wear.
2. It has been used in various industries at macro level.
3. Electro-chemical machining can be used effectively for micro machining components by suitable tool design and process control.
4. Electrochemical machining uses direct current with the current applied continuously.

This project proposes a new approach of μECM, which uses pulsed current and a feedback loop. The advantages of pulsed current are that it aids in the effective removal of metal ions between anode and cathode and it offers good control of the etched surface. The feedback loop is to be designed in such a way that the system detects variations in the current in machining zone and automatically compensates for them.

1.1. OBJECTIVES AND SCOPE

The main objectives of this study would be:

1. Develop model for material removal rate (MRR) for μECM.
2. Design a system for micro machining.
3. Compare open loop/closed loop results.
4. Predict the system behavior and compare with measured data.

The scope of this project would be:

1. Utilize copper alloy (CA 173) and stainless steel (SS316L).

2. Fabricate simple round holes.

3. Apply to micro deburring.

4. Use a fixed concentration of sodium nitrate ($NaNO_3$) as electrolyte.

2. LITERATURE REVIEW

Electrochemical machining removes material from an electrically conductive workpiece. The basis of this process is electrolysis, which is governed by the laws established by Faraday.

2.1. ELECTROLYSIS

Electrolysis is the chemical reaction that occurs when an electric current is passed between two conductors dipped in a liquid solution. The completeness of this electric circuit is found by attaching an ammeter to the system and ammeter displays a reading. The liquid solution conducts electricity because otherwise the circuit would be incomplete. A schematic of an electrolytic cell utilizing copper sulphate as an electrolyte and copper wire as electrodes appears in Figure 1.

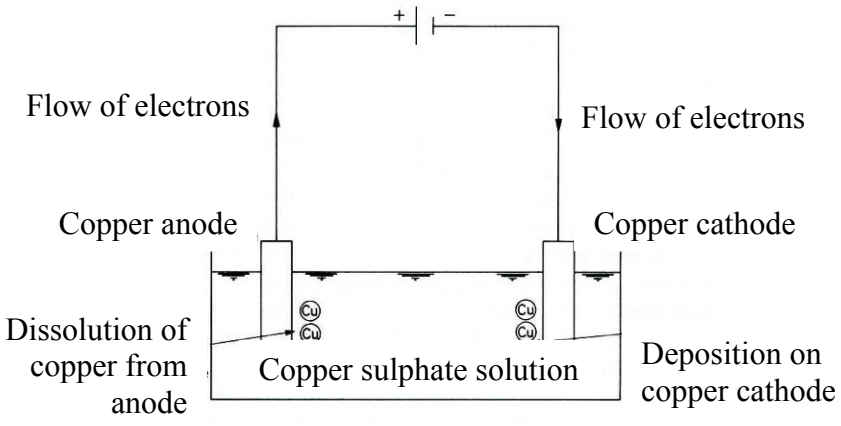

Figure 1

Schematic of electrolysis (McGeough 2005)

The chemical reactions are named anodic reactions or cathodic reactions depending on whether they occur at the anode or cathode, respectively. The major difference between electrolytes and metallic conductors of electricity is that current is carried by electrons in metals whereas it is carried by ions in electrolytes. Ions are nothing but atoms that have either lost or gained electrons and thereby acquired a positive or negative charge. The positively charged ions travel towards the cathode and the negatively charged ions travel towards the anode. Since the electrolyte must be neutral, there must be a balance between the total positive charge and the negative charge. At the end of the reaction, the amount of material lost by one of the electrodes is equal to the amount of material gained by the other. Hence, this process can be used for both material removal and addition. The major applications of electrolysis are electroplating and electro-polishing (McGeough 2005).

2.2. ELECTROCHEMICAL MACHINING

Electrochemical machining is a material removal process similar to electro polishing. In this process the workpiece to be machined is made the anode and the tool is made the cathode of an electrolytic cell with a salt solution being used as an electrolyte. The tool is normally made of copper, brass, or stainless steel. The tool and the workpiece are located so there is a gap between 0.1mm to 0.6mm between them (Rajurkar et al. 1999). The tool is designed so that it is the exact inverse of the feature to be machined. On application of a potential difference between the electrodes and subsequently when adequate electrical energy is available between the tool and the workpiece, positive

metal ions leave the workpiece. Since electrons are removed from the workpiece, oxidation reaction occurs at the anode which can be represented as,

$$M \rightarrow Mn^{+} + ne^{-} \quad (1)$$

where n is the valence of the workpiece metal. The electrolyte accepts these electrons resulting in a reduction reaction which can be represented as,

$$nH_2O + ne^{-} \rightarrow \frac{n}{2} H_2 + nOH^{-} \quad (2)$$

Hence the positive ions from the metal react with the negative ions in the electrolyte forming hydroxides and thus the metal is dissoluted forming a precipitate. The electrolyte is constantly flushed in the gap between the tool and the workpiece to remove the unwanted machining products which otherwise would grow to create a short circuit between the electrodes. The electrolyte also carries away heat and hydrogen bubbles. The tool is advanced into the workpiece to aid in material removal (McGeough 2005). A schematic of a cell used for electrochemical machining is shown in Figure 2.

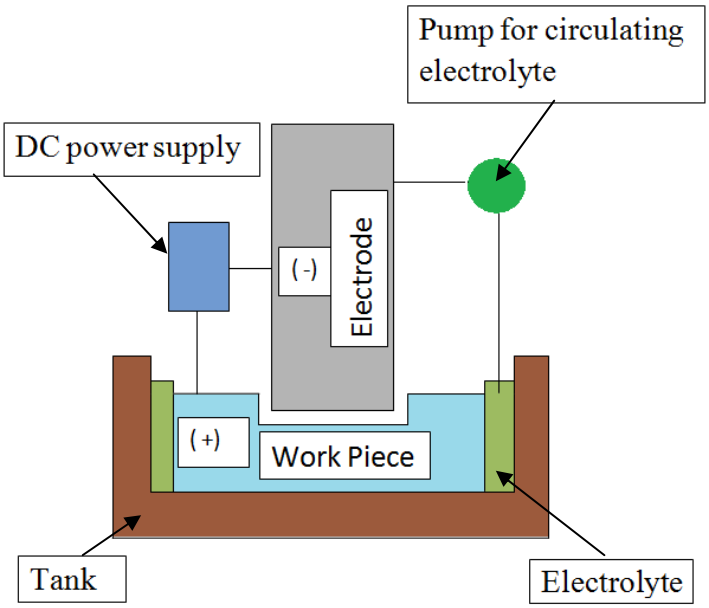

Figure 2

Schematic of ECM

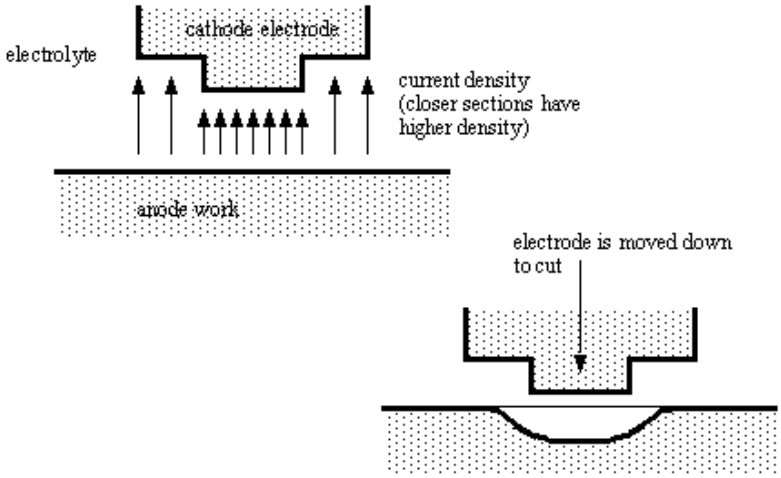

Figure 3

Material removal in ECM (Jack 2001)

A pump system must filter the electrolyte and circulate it because the electrolyte carries away machining waste. A schematic of material removal as the tool advances into the workpiece is shown in Figure 3.

There are several process configurations that can be selected based on the requirements and the capabilities of the machine. The various configurations are:

1. Both the tool and the workpiece are stationary.
2. The tool is given linear and rotary motion while the workpiece is stationary.
3. Both the tool and the workpiece move.

2.2.1. Advantages of Electrochemical Machining

Electrochemical machining offers several advantages over other competing technologies. These advantages have made ECM the best choice for a variety of applications.

The advantages:

a. No tool wear as non contact working mode avoiding problems such as elastic deformation, vibration and breakage (Rajurkar et al. 2006).
b. High material removal rate.
c. Ability to machine a wide variety of materials without affecting microstructure or surface properties.
d. No heat generated during machining.
e. Cutting, drilling, deburring and shaping possible.
f. Ease of machining complex features.
g. Stress free machined surface.

h. Environmentally acceptable.

2.2.2. Applications of Electrochemical Machining

Electrochemical machining finds majority of its applications in deburring, hole drilling and shaping.

2.2.2.1. Deburring

Burrs are undesirable in any machined workpiece but are at the same time inevitable. Deburring the machined components manually is a time consuming process and also not effective (McGeough 2005). Electrochemical machining with its inherent advantages is a suitable choice for deburring. A flat faced tool is used to remove the surface asperities on the workpiece. As the tool is moved slowly towards the workpiece surface it encounters the burrs first. Since the tool is relatively large in comparison to the burrs and the current densities are high at the peaks of the burrs, they are machined first. This is a fast process and simple to control. The current densities at the cathode and at the peak of the burrs as machining progresses are shown in Figure 4.

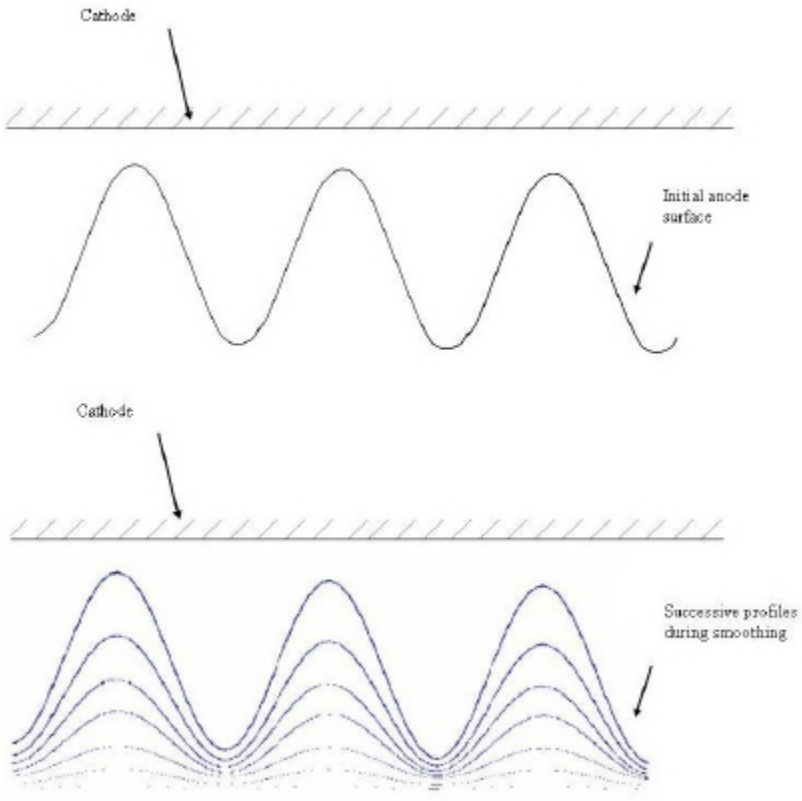

Figure 4

Current densities at the cathode and the burrs (McGeough 2005)

2.2.2.2. Hole Drilling

Electrochemical machining can be used to machine either a single hole or a series of holes with the same characteristics. The tool is designed so that there is electrolyte flow both around and along the length of the electrode or through a hole inside the electrode so that the precipitates flow out. Flushing the precipitates is crucial in hole drilling because otherwise the removed material would pile up and form a short circuit. Most of the material is removed in the gap between the bottom of the tool and the workpiece; however the high current densities at the tip of the cathode removes some

material at the sides of the cathode as the tool progresses into the workpiece. This enlarges the hole because further material leaves as the tool progresses into the workpiece. This can be overcome by coating the tool sides with an insulating material so that machining occurs only at the tool base or tip. Since the hole shape depends on the stationary cathode's shape, the holes drilled need not be round (McGeough 2005). The position of the tool and the flow path of the electrolyte in a hole drilling operation are shown in Figure 5.

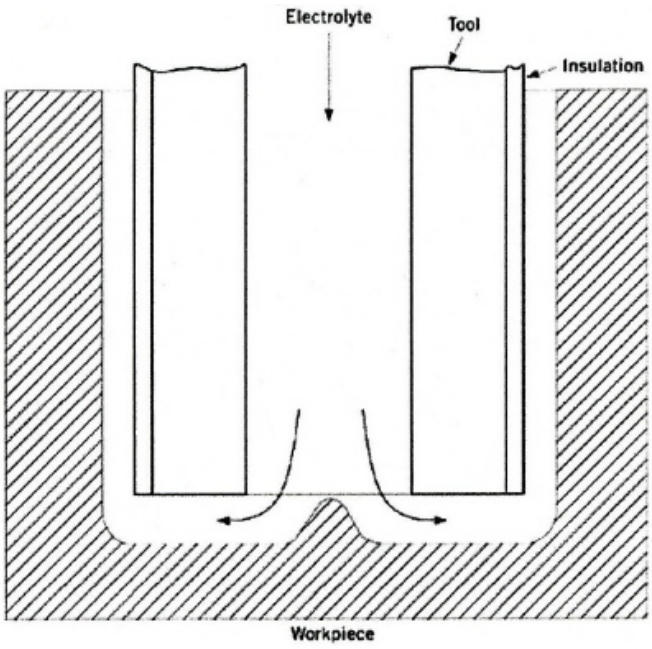

Figure 5

Hole drilling using ECM (McGeough 2005)

Since material is removed radially in ECM the tool must compensate for this removal. Figure 6 shows the expected cavity shape to be formed with the given tool and the shape finally obtained.

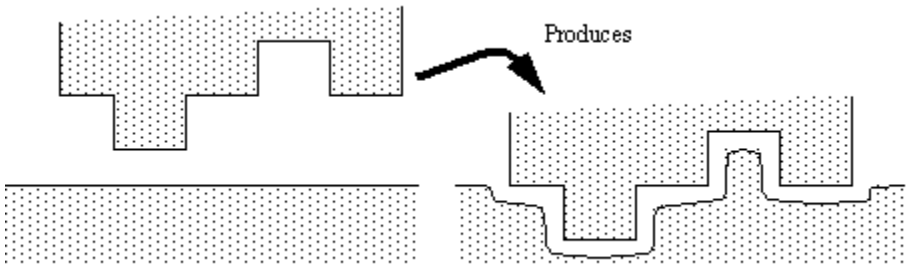

Figure 6

Shape of tool and cavity formed after machining (Jack 2001)

Figure 7

Holes drilled in a turbine nozzle block using ECM (Barber-Nichols Inc. 2008)

Holes drilled in a turbine nozzle block by ECM are shown in Figure 7. The holes were machined at different angles.

2.2.2.3. Shaping

In this process a constant gap is maintained between the tool and the workpiece as the tool progresses into the workpiece. In contrast to other processes the electrolyte flow is all over the workpiece. This process is mainly used to manufacture turbine blades as the blades can be placed close to each other increasing the efficiency of the turbine. Figure 8 shows turbine blades machined using ECM.

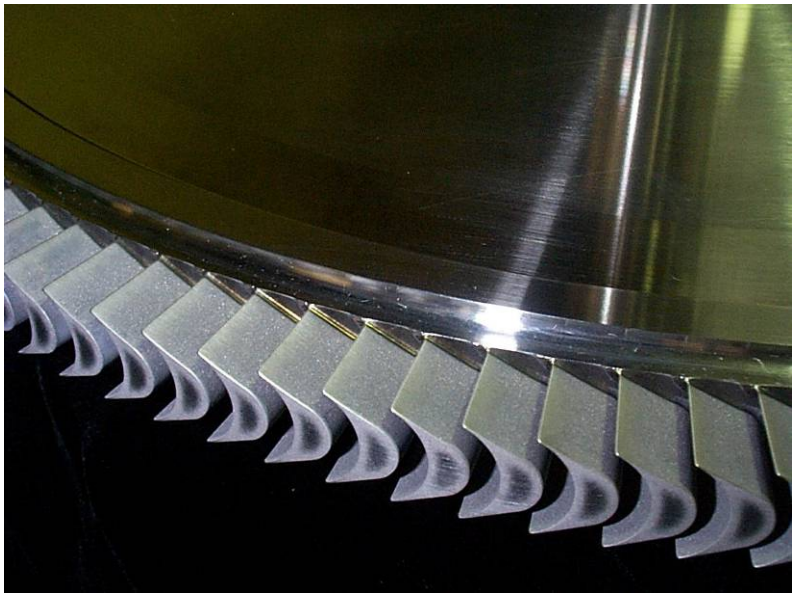

Figure 8

Turbine blades machined using ECM (Barber-Nichols Inc. 2008)

2.3. ELECTROCHEMICAL MICRO MACHINING

The shaping of parts with dimensions in the range of 5 to 500 μm and production of parts with high surface finish has a lot of applications in industries (Rajurkar et al. 1999). The fabrication of microstructures by ECM is known as μECM. Alternately, it can be thought of as a material removal process maintaining micron range tolerances. The removal of material occurs atom by atom from the workpiece surface. The semi-conductor industry requires the machining of components of complex shape in high strength alloys (Hocheng et al. 2003). Electrochemical micro machining is the key technology for the semiconductor, electro communication, optics, medicine, bio technology; automotive, avionics, and ultra precision machinery industries. This technique has replaced the chemical etching process which was predominantly being used in these industries because of the many advantages it offered. This process does not induce any stress into the workpiece or form micro cracks and ridges which are inevitable in other thermal processes. Micro fabrication by μECM can be done through mask or mask less techniques (Rajurkar et al. 1999). This technique requires a better degree of tooling and process control compared to the conventional ECM technique. The selection of electrolyte is very critical because of the extremely small gap between the tool and the workpiece. Electrochemical micro machining is still in its initial stages and lot of research needs to be done to improve material removal, surface quality, and accuracy by optimizing the various process parameters (Bhattacharyya, Malapati, and Munda 2005). Though ECM has a lot of scope for micro machining there are a number of technical issues that need to be addressed such as stray material removal, tool

structure , and machining gap (Rajurkar et al. 1999).

Surface finishing can also be controlled by μECM because it removes material at the micro level. This technique was employed in the manufacturing of micro nozzles (Rajurkar et al. 1999).

2.4. THEORY OF ELECTROCHEMICAL MACHINING

2.4.1. Material Removal Rate

The amount of material removed is determined by Faraday's first law which states that the mass of the substance removed at an electrode is proportional to the quantity of current passed to that electrode. So,

$$V = CIt \tag{3}$$

where,

V = volume of metal removed (mm^3)

C = electrochemical constant (mm^3/amp-s)

I = current (amps)

t = time (sec)

The electrochemical constant is unique for every work material and given by Equation 4.

$$C = \frac{A_w}{ZF\rho} \tag{4}$$

where,

A_w = molecular mass

Z = number of valence electrons

F = Faraday's constant

ρ = density of work material

Ohm's Law states that the current

$$I = E / R \tag{5}$$

where,

E = voltage

R = resistance

The resistance R for ECM operations is given as,

$$R = \frac{gr}{A} \tag{6}$$

where,

g = gap between the tool and the workpiece (mm)

r = resistivity of the electrolyte (ohm-mm)

A = surface area of tool (mm^2)

Hence, MRR is given as,

$$MRR = \frac{V}{t} = \frac{CEA}{gr} \tag{7}$$

These equations were derived assuming 100% efficiency (Groover 2006).

2.4.2. Rate of Machining

The rate at which different metals can be machined depends on the amount of current passed and the duration for which it is passed. This is an indirect way of expressing the statement that the rate at which the material is removed is dependent on the rate of reaction according to Faraday's Law. The behavior of the anodic workpiece in the particular electrolyte chosen also affects the rate of the reaction. The factors that affected the rate of machining were type of electrolyte, flow rate of electrolyte, temperature of electrolyte, and its pH value (Bhattacharyya and Munda 2003). The table on which the machining setup is established needs to be extremely stable. When there is no sufficient electrolyte flow, the machining products are not swept away which affects further machining.

2.4.3. Geometry, Condition, and Accuracy of Machined Surface

The geometry, condition, and accuracy of the machined surface depended on the electrolyte salt type and concentration, machining gap, pulse power supply setting, flow velocity, and flow profile (Stofesky 2006). μECM is capable of producing surfaces free of any metallurgical alterations. It was observed that nickel based, cobalt based , and stainless steel alloys produce smoother surface (0.13 to 0.38 μm Ra) compared to surface finish obtained on iron based alloys and steel (0.63 to 1.52 μm Ra). Surface finish was governed by the mass transport at the anode. A better surface finish was obtained on workpieces with fine grained structure (Rajurkar et al. 2006). An electro polished surface was obtained when dissolution occurred at or beyond the limiting current. An etched and rough surface was obtained when machining occurred below the

limiting current. The anodic limiting current density, i_l, for a reaction controlled by convective mass transport is given by Equation (8).

$$i_l = nFD\frac{C_{sat}}{\delta} \tag{8}$$

where D is the effective diffusion coefficient that takes into account the contributions from transport by migration, C_{sat} is the surface concentration, n is the apparent dissolution valence, F is the Faraday constant, and δ is the diffusion-layer thickness. The apparent dissolution valence number is determined using Equation (9).

$$n = \frac{ItM}{\Delta WF} \tag{9}$$

where I is the current, t is the dissolution time, ΔW is the anodic weight loss, M is the molecular weight of dissolved material. The anodic diffusion layer thickness depends on hydrodynamic conditions and is given by

$$\delta = \frac{L}{Sh} \tag{10}$$

where L is a characteristic length and Sh is the Sherwood number that represents non-dimensional mass transport rate (Datta 1998).

Formation of salt films at limiting or higher current densities led to micro finishing. The formation of oxide films on the work surface impeded further machining resulting in a rough surface. The gas generated at the anode needed to be swept away which otherwise generated bubbles resulting in a pitted surface. Increasing the current

density and electrolyte velocity had also resulted in a smooth surface. Accuracy and dimensional control were dependent on the electrolyte being used. The current density characteristic of the electrolyte being used affected the accuracy of the components (Datta and Romankiw 1989).

2.5. PROCESS PARAMETERS

The main process parameters governing the ECM process are electrolyte, current, and voltage settings, electrode gap and flow velocity.

2.5.1. Electrolyte

The electrolyte is one of the main components of the machining system. The electron movement from the cathode to the anode is dependent on the properties of the electrolyte. The electrolyte conductivity in the gap between the cathode and the anode was dependent on the following parameters: the starting electrode distance, concentration of salt in the solution, local hydroxide concentration in electrolyte, bulk and local temperature, electrolyte flow rate, and the velocity of electrolyte (Stofesky 2006). High flow rates of electrolyte were not desirable as they caused tool erosion. Surface brightening was achieved only under conditions where the dissolution mechanism was independent of structure. One of the main considerations in the design of the tool is that it should provide the desired agitation of the electrolyte (Datta and Landolt 2000). The control of electrolyte speed and flow direction was important for the machining process to continue. It is a difficult task to maintain the flow of electrolyte in the extremely small gap without affecting the tool stability (Rajurkar et al. 2006).

Electrolyte removes the machining products generated at the electrodes and dissipates the heat generated. Machining performance is governed by the behavior of anodic workpiece in a given electrolyte. In micro machining because of the small gap between the tool and the electrode, the density of current is very high which results in vaporization of the electrolyte. The electrolyte must be chosen in such a way that it does not vaporize and carries the machining products away from the workpiece. Table 1 shows the electrolytes that can be used for various alloys in order to achieve the best results.

Table 1

Electrolytes for different alloys (Jack 2001)

Alloy	Electrolyte
Iron based	Chloride solutions in water
Ni based	HCl or mixture of brine and H_2SO_4
Ti based	10% HF + 10%HCl + 10%HNO_3
Co-Cr-W based	NaCl
WC based	Strong alkaline solutions

The main functions of the electrolyte are to provide the ideal conditions for the dissolution of the workpiece material, conduct electricity, carry away the unwanted machining products and heat generated, and maintain a constant temperature in the

machining gap. The accumulation of reaction products at anode and cathode was undesirable as they reduced the specific conductivity of the electrolyte. There was a high probability of the electrolyte being boiled by the power transmitted across the gap and this led to machining being stopped in an abrupt manner (Kirk-Othmer 2004). Electrolytes need to satisfy certain requirements so that they can be used effectively for μECM process (University of Nebraska Lincoln 2008).

1. The cations and the anions present in the electrolyte should be such that the anions permit the dissolution of the workpiece without forming a film on its surface and the cations do not deposit on the tool. The anions mostly used are chlorides, sulphates, nitrates, and hydroxides.
2. The electrolyte needs to have a high conductivity and low viscosity so that it is able to flow easily in the narrow gap between the tool and the workpiece.
3. The electrolyte should be such that it is non toxic, safe to use, and does not erode the machine. Neutral salt solutions are most commonly used as electrolytes.
4. The electrolyte should be cheap and readily available and should not exhibit large variations in its properties as the machining progresses.

The selection of an electrolyte for a particular application depends on the following considerations:

1. The nature of the workpiece material.
2. Surface finish and dimensional tolerance requirements.
3. Productivity expected.

The electrolytes used in electrochemical machining can be broadly classified into two categories:

1. Passive electrolyte.
2. Non - passive electrolyte.

Passive electrolytes contain oxidizing anions such as sodium nitrate and non-passive electrolytes contain aggressive anions such as sodium chloride. Passive electrolytes are known to give better machining precision due to formation of oxide films and oxygen evolution in stray current region (Datta and Romankiw 1989).

The electrolyte in the electrolytic cell could be divided into two zones, one near the electrode surface where a stagnant diffusion layer existed in which there was no convection and the other zone was the bulk solution where no concentration gradient existed because of perfect mixing. The current convection conditions existing in the solution affected the thickness of the stagnant diffusion layer. The thickness was estimated from dimensionless mass transport relations (Datta and Landolt 2000).

The most commonly electrolytes are sodium chloride and sodium nitrate. The relationship between current efficiency and current density varies for each electrolyte and this relationship ultimately governs the material removal rate. Sodium nitrate is preferred over sodium chloride because at small gaps, the current density and the current efficiency are high resulting in a higher material removal rate where as at large gaps the current density and efficiency are low resulting in a low material removal rate. The electrolyte concentrations commonly used range from around 30 g/L to 35 g/L and a pH of around 7 that can enhance the dissolution of metal without affecting the micro tool.

By using an electrolyte with a lower concentration, inter electrode gap could be reduced resulting in improved accuracy (Bhattacharyya, Malapati, and Munda 2005).

The particular method chosen for supplying electrolyte to the machining gap depends on the process configuration. There are many ways by which the electrolyte can be supplied (University of Nebraska Lincoln 2008).

1. The electrolyte is supplied continuously and allowed to flow through the gap and on the workpiece.
2. The electrolyte is supplied through a capillary in the tool so that it flushes away the machining products.
3. The tool and the workpiece are sprayed with an electrolyte continuously.

Da Silva Neto et. al.(2000) reported that sodium chloride resulted in higher material removal rate compared to sodium nitrate when machining SAE-XEV-F valve steel with copper electrode. Sodium nitrate is a non-passivating electrolyte and the current efficiency was almost constant during machining (Datta 1993) and hence has a higher material removal rate. The MRR of sodium nitrate and sodium chloride are compared in Figure 9.

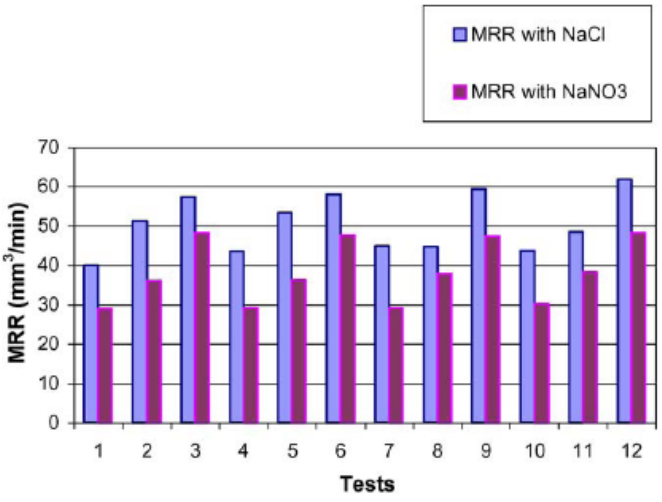

Figure 9

Comparison of MRR for different electrolytes during machining of SAE-XEV-F valve steel (Da Silva Neto et al. 2000)

2.5.2. Current and Voltage

Current density depended on the rate at which ions arrived at respective electrodes which was proportional to the applied voltage, concentration of electrolyte, gap between the electrodes, and tool feed rates. As the tool approached the work, the length of the conductive current path decreased and magnitude of current increased. This lessening of the gap and increase in current continued until the current was just sufficient to remove the metal at a rate corresponding to the rate of tool advance. The total amperage required for machining of the workpiece could be calculated by multiplying the current density and the surface area being machined. When the equilibrium gap approaches zero value, overvoltage approached applied voltage. Overvoltage (ΔV) was calculated by Equation (11) at various equilibrium gap for a given valency.

$$\Delta V = V - \frac{\rho ZF}{KA} Y_e f \tag{11}$$

where V is the Voltage, K is the conductivity, ρ is the density, Y_e is the equilibrium gap, Z is the valency, f is the feed rate, and A is the atomic weight. Overvoltage was a parameter which restricted material removal rate and was sensitive to tool feed rate and equilibrium machining gap. The plot of overvoltage versus current density during machining an aluminum sheet using brass cathode with 1.5M sodium chloride electrolyte is given in Figure 10. The parameters for the plot were A = 26.97, Z = 3, V = 40V, F = 96500, K = 0.184 $Ohm^{-1}cm^{-1}$, T= 20°C, and f = 0.000667 cm/s (Mukherjee, Kumar, and Srivastava 2005).

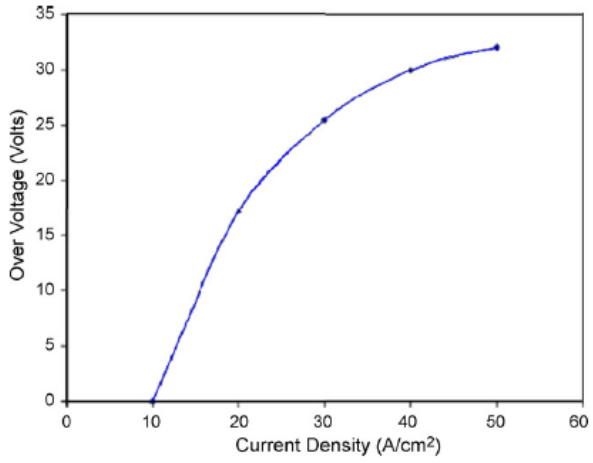

Figure 10

Plot of current density versus over voltage for aluminum (Mukherjee, Kumar, and Srivastava 2005)

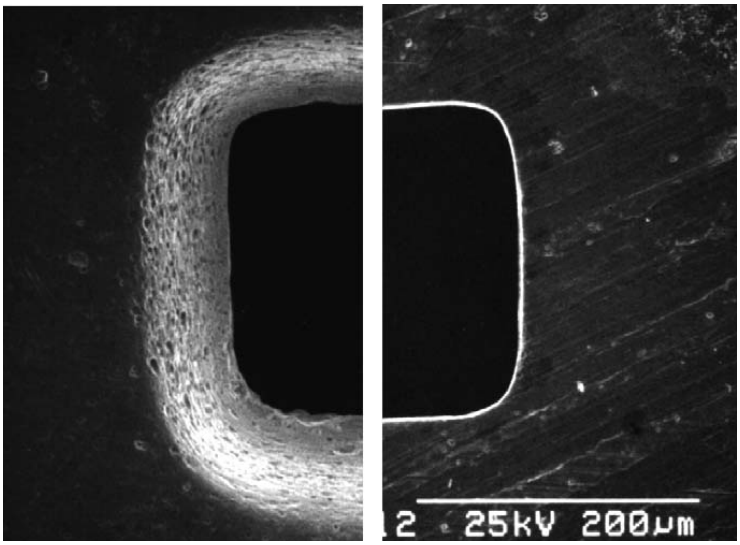

(a) (b)

Figure 11

Comparison of insertion and exit side of hole drilled in 0.2mm Ni plate

(a) View from insertion side (b) View from exit side (Kurita et al. 2006)

As machining voltage increased, the machining speed increased. The machining speed reached its maximum value at a particular voltage and decreased because electrode surface was gradually covered by bubbles generated at increased voltage. Constant voltage power supply caused problems like over current. Current increased as depth of hole increased and removal of hole side surface was accelerated. Difference of hole shape at insertion and exit side became large (Kurita et al. 2006) as shown in Figure 11.

A 0.2 mm diameter Ni rod was used as cathode and a 0.2 mm thick Ni plate was used as the work piece. The parameters for the experiments were:

Machining voltage: 16 V

Pulse-on time: 32 ms

Pulse-off time: 57 ms

Amplitude of flushing out: 710 mm

Electrolyte concentration: 3.5 g/dm^3 $NaClO_3$

The machining speed and side gap were calculated and analyzed. The machining speed was calculated by dividing the work piece thickness by the time for penetration. The side gap was defined as one half the difference between the diameter at exit and the tool diameter. The relationship between machining speed and side gap versus machining voltage is shown in Figure 12. It was observed that the machining speed increased with increase in machining voltage. The machining speed decreased with increase in voltage after a particular value because the electrode surface was covered with bubbles.

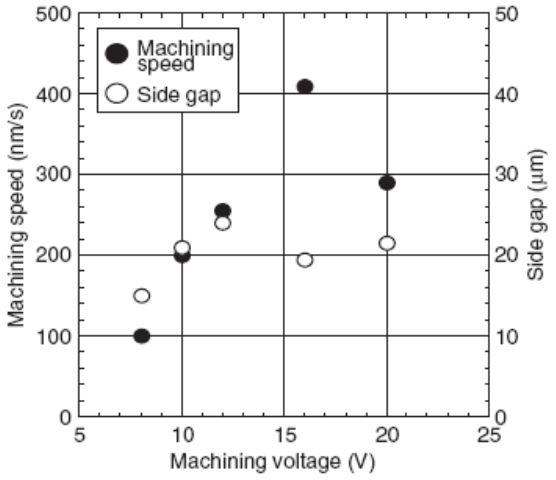

Figure 12

Machining speed and side gap versus machining voltage (Kurita et al. 2006)

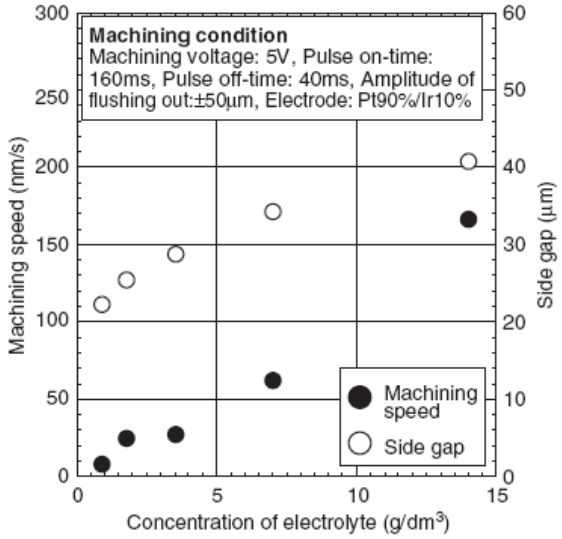

Figure 13

Machining speed and side gap versus electrolyte concentration (Kurita et al. 2006)

The relationship between machining speed and side gap for various electrolyte concentrations is given in Figure 13. It was observed that the machining speed and side gap increased with electrolyte concentration. The larger machining gap led to lower accuracy.

It was observed that a power supply which maintained a constant current throughout the machining process was the most effective for electrochemical machining (Kurita et al. 2006). The plot of machining speed and side gap versus machining current is shown in Figure 14.

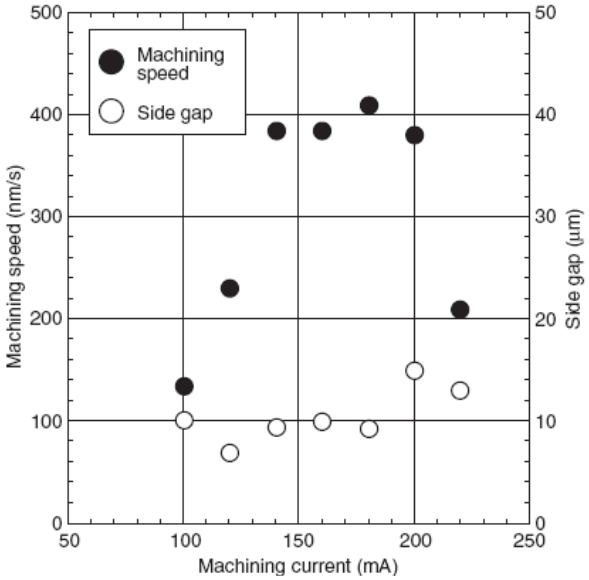

Figure 14

Machining speed and side gap versus machining current (Kurita et al. 2006)

The functional relationship between the potential just outside the double layer and that in the metal must be known in order to calculate potential distribution in the electrolyte and the corresponding current distribution on the electrode. Double layer is a structure that appears on the surface of the electrode when it is placed in the electrolyte. Transport mechanisms responsible for anodic leveling played a crucial role in ECM because they controlled the shape and surface finish that could be achieved (Datta and Landolt 2000). Bhattacharyya, Malapati, and Munda (2005) reported that 3 Vpp machining voltage, 55 Hz frequency and 20 g/l sodium nitrate electrolyte concentration were effective parameters that could enhance accuracy of μECM with highest amount of material removal. The effect of voltage on material removal is shown in Figure 15. A

Ø600 µm stainless steel electrode was used with a 150 µm thick copper sheet with 30 g/l sodium nitrate electrolyte.

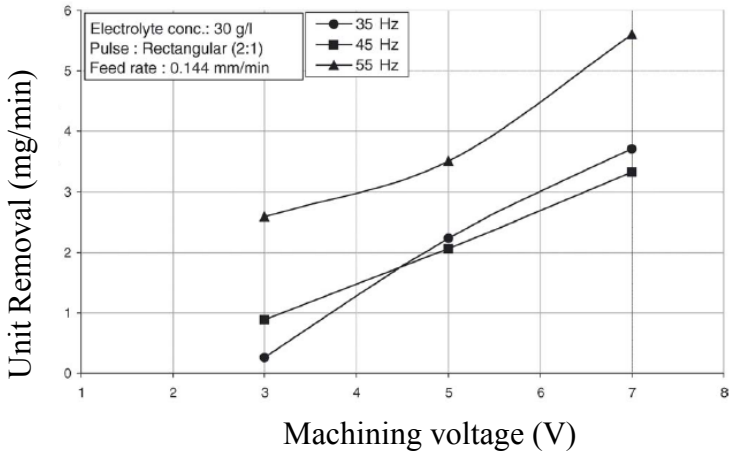

Figure 15

Influence of machining voltage on unit removal (Bhattacharyya, Malapati, and Munda 2005)

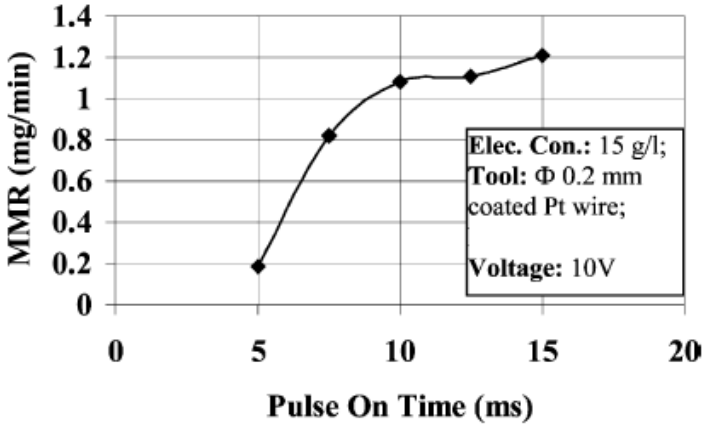

Figure 16

Influence of pulse ON time on MRR (Bhattacharyya and Munda 2003)

It was observed that the MRR increased for increased pulse ON time indicating that the MRR was higher at lower frequencies as shown in Figure 16 (Bhattacharyya and Munda 2003). Examination of SEM micrographs indicated that low voltage, moderate electrolyte concentration, and high frequency which was around 60 Hz in this case could enhance the accuracy of the process.

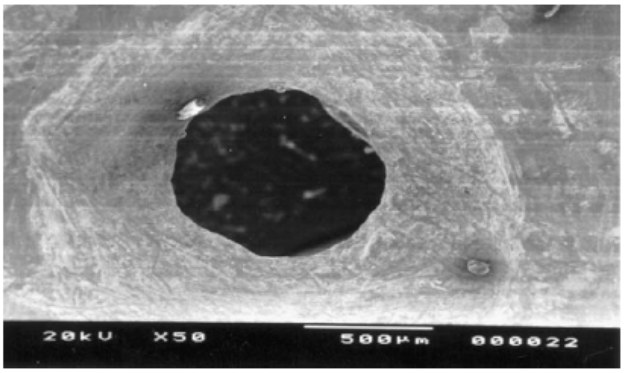

Figure 17

SEM micrograph of hole drilled on copper workpiece with Pt electrode (Bhattacharyya and Munda 2003)

Figure 17 shows a SEM micrograph of a hole drilled in 0.4 mm thick copper plate with a Ø200 µm platinum electrode. The sidewalls of the electrode were coated with silicon nitride by chemical vapor deposition. The parameters were 50 Hz, 25 g/l sodium nitrate electrolyte, and 10 Vpp machining voltage (Bhattacharyya and Munda 2003).

Equation 12 as proposed by Mount, Eley, and Clifton (2000) gives the current I across the electrolyte.

$$I = \frac{\kappa(V - V_o)A}{z} \tag{12}$$

where κ is the electrolyte conductivity, V is the applied voltage, V_o is the portion of applied voltage required to drive machining process, A is the electrode area , and z is the gap between the electrodes.

It was assumed that all this current led to electrode dissolution and hence the dissolution current I of the workpiece given as,

$$I = \left[\frac{nFA\rho}{M}\right]\frac{dy}{dt} \tag{13}$$

where n is valency, F is Faraday's constant, ρ is density of workpiece material, M is molecular mass of workpiece , and $\frac{dy}{dt}$ is erosion rate .

2.5.3. Electrode Gap

The gap between the tool and the workpiece must be in the range of tens of microns. The length of electrode and its position with respect to the workpiece determined the gap between the electrodes. As the gap became larger higher voltages were required to maintain the correct current density. The higher voltages resulted in wider profiles of drilled holes. If the gap was too small, the voltage dropped to a low value which resulted in narrow machined features. There was no proper electrolyte flow if the gap became low. The inter electrode gap needed to be maintained precisely as any abnormal status led to unwanted machining results (Rajurkar et al. 2006). Kim et al.

(2005) had shown that the machining gap increased as the machining time increased, and the gap of initially machined layer (g_1) was larger than that of layer currently being machined (g_0). The difference (g_1-g_0) was estimated to be less than 10 microns when machining 300 µm thick stainless steel plate with Ø20 µm tungsten carbide electrode. The electrolyte was 0.1M sulphuric acid ($H_2SO_{4)}$ and machining voltage was 6 V. Figure 18 shows the plot of machining gap versus time. This difference in the machining gap resulted in a tapered side wall.

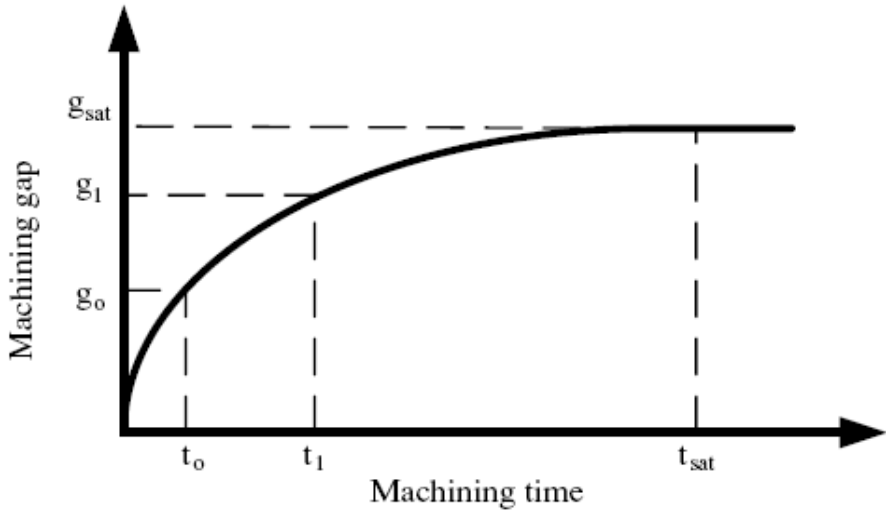

Figure 18

Plot of machining gap versus time (Hyun Kim et al. 2005)

The variation of machining gap for different concentrations of the electrolyte is shown in Figure 19. As the electrolyte concentration was decreased the machining gap decreased but machining was unstable at very low concentration (Kim et al. 2005).

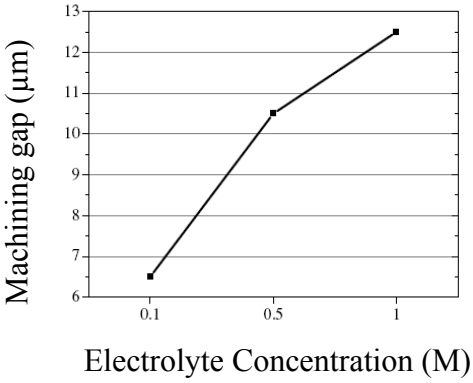

Figure 19

Variation of machining gap with electrolyte concentration (Kim et al. 2005)

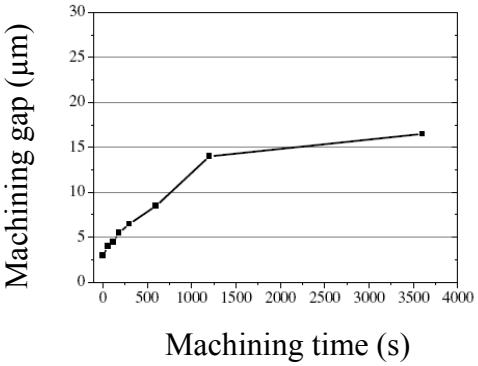

Figure 20

Variation of machining gap with machining time (Hyun Kim et al. 2005)

The variation of machining gap with machining time is shown in Figure 20. It was observed that the dissolution was high in the initial stage of machining but decreased with time.

Equation 14 proposed by Kozak, Rajurkar, and Makkar (2004) gives the equilibrium gap size S_f in a steady state ECM process.

$$S_f = \kappa K_V \frac{U - E}{V_f} \tag{14}$$

where κ is the electrolyte conductivity, K_V is the electrochemical machinability coefficient defined as volume of material dissolved per unit electrical charge, U is the working voltage, E is the total over potential of electrode processes, and V_f is the feed rate of electrode.

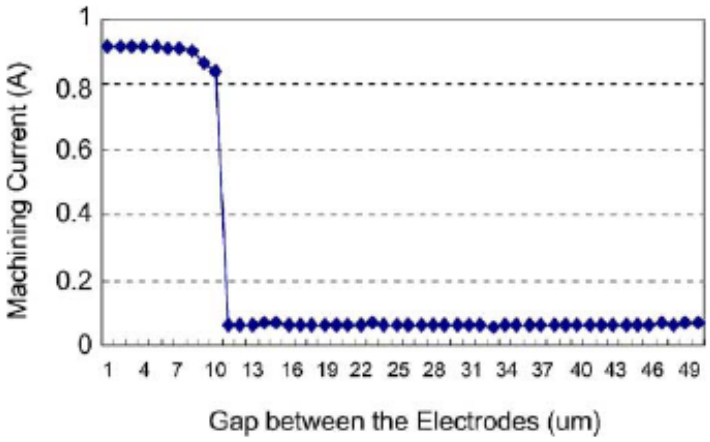

Figure 21

Current behavior with inter electrode gap (Yong et al. 2003)

A plot of machining current versus inter electrode gap is shown in Figure 21. The parameters for the plot were : Ø200 µm copper electrode, stainless steel workpiece, 10% $NaClO_3$ solution as electrolyte, and 5 V working voltage.

2.5.4. Flow Rate

Although the material removal rate is dictated by the reaction rate, the flushing away of the reaction products away from the machining zone is also important for efficient machining. The selection of the ideal flow patterns and velocity was paramount for obtaining the best results. The gradient in the flow path directly affected the surface finish and depth of cut (Stofesky 2006).

3. MODELING

The existing formulae for material removal rate are for electrochemical machining using direct current. A model was developed for the calculation of material removal rate while using pulsed current.

3.1. MODEL FOR MATERIAL REMOVAL RATE

The developed model gives the volume of material removed for each pulse of current. The model was derived under the assumption that material is removed only during the pulse ON duration and flow rate is adequate to flush away the reaction products. Equation (15) gives the volume of material removed V_u for each pulse.

$$V_u = \int_0^{\tau} \frac{CEAdt}{gr} \tag{15}$$

where,

C = electrochemical constant = $\frac{A_w}{ZF\rho}$

E = voltage

A = electrode area

g = tool/substrate gap

r = *e*lectrolyte resistivity

τ = pulse duration

The MRR was calculated using Equation 16.

$$MRR = \frac{V_u}{\tau} \tag{16}$$

where V_u is the volume of material removed for one pulse and τ is the pulse duration. The pulse duration was calculated from the oscilloscope.

3.2. CALCULATION OF ELECTROCHEMICAL CONSTANT

The formula for calculating electrochemical constant for single material elements was given in Equation (4).

$$C = \frac{A_w}{ZF\rho}$$

The electrochemical constant for alloys was calculated using Equation 17 (Jack 2001).

$$C = \frac{100}{\sum_i \left(\frac{x_i z_i}{A_i} \right) \rho F} \tag{17}$$

$$\rho = \frac{100}{\sum_i \left(\frac{x_i}{\rho_i} \right)} \tag{18}$$

where ρ is the density of the alloy, F is the Faraday's constant, x_i is the percentage of i^{th} element in the alloy, z_i is the valence of i^{th} element in the alloy, A_i is the atomic weight of i^{th} element in the alloy, and ρ_i is the density of the i^{th} element in the alloy.

3.2.1. Calculation of Electrochemical Constant for CA-173:

The composition of CA-173 alloy is given in Table 2 (ASTM B196, 2007).

Table 2

Composition of CA-173 alloy (ASTM B196, 2007)

ELEMENT	**PERCENTAGE (%)**	**VALENCY**	**ATOMIC MASS (g/mole)**	**DENSITY (g/cm^3)**
Copper (Cu)	97.7	2	63.57	8.96
Beryllium (Be)	1.9	2	9.012	1.848
Lead (Pb)	0.4	2	207.2	11.34

Applying Equations (17-18)

$$\rho_{CA-173} = \frac{100}{\frac{97.7}{8.96} + \frac{1.9}{1.848} + \frac{0.4}{11.34}} = \frac{100}{10.9 + 1.028 + 0.035}$$

$$= \frac{100}{11.963} = 8.36 \frac{g}{cm^3}$$

$$C_{CA-173} = \frac{100}{\left(\frac{97.7*2}{63.57} + \frac{1.9*2}{9.012} + \frac{0.4*2}{207.2}\right)*8.36*96500}$$

$$= 3.54*10^{-2} \frac{mm^3}{A.s}$$

3.2.2. Calculation of Electrochemical Constant for SS-316L:

The composition of SS-316L is given in Table 3 (ASTM A 240, 2007).

Table 3

Composition of SS-316L alloy (ASTM A 240, 2007)

ELEMENT	**PERCENTAGE (%)**	**VALENCY**	**ATOMIC MASS (g/mole)**	**DENSITY(g/cm^3)**
Iron (Fe)	68.2	2	55.85	7.86
Chromium (Cr)	17.2	2	51.99	7.19
Nickel (Ni)	10.9	2	58.71	8.9
Molybdenum (Mo)	2.1	3	95.94	10.28
Manganese (Mn)	1.6	2	54.94	7.43

Applying Equations (17-18)

$$\rho_{SS-316L} = \frac{100}{\frac{68.2}{7.86}+\frac{17.2}{7.19}+\frac{10.9}{8.9}+\frac{2.1}{10.28}+\frac{1.6}{7.43}}$$

$$= \frac{100}{8.676+2.392+1.224+0.204+0.215}$$

$$= \frac{100}{12.711} = 7.86\frac{g}{cm^3}$$

$$C_{SS-316L} = \frac{100}{\left(\frac{68.2*2}{55.85}+\frac{17.2*2}{51.99}+\frac{10.9*2}{58.71}+\frac{2.1*3}{95.94}+\frac{1.6*2}{54.94}\right)*8.36*96500}$$

$$= 3.68*10^{-2}\frac{mm^3}{A.s}$$

3.3. CALCULATION OF ELECTROLYTE RESISTIVITY

The electrolyte resistivity was measured in an indirect way. The conductance of the electrolyte was found using Thermo Orion micro electrodes conductivity probe. The conductance measured was 29.9 millisiemens. The conductivity was calculated using Equation (19).

$$Cell\ Conductance * Cell\ Constant = Conductivity \quad (19)$$

The cell constant value was obtained from equipment manual to be 1 cm^{-1}. The conductivity obtained using Equation (19) is 0.0299/Ω-cm. The resistivity was measured as,

$$Resistivity = \frac{1}{Conductivity} = 33.44 \ \ \Omega cm$$

3.4. MODEL FOR DEBURRING

A model was developed which enabled to calculate the time and speed of electrode necessary to deburr a flat component. The burrs on the surface after micro electric discharge machining (μEDM) were in the form of small hemispheres as shown in Figure 22.

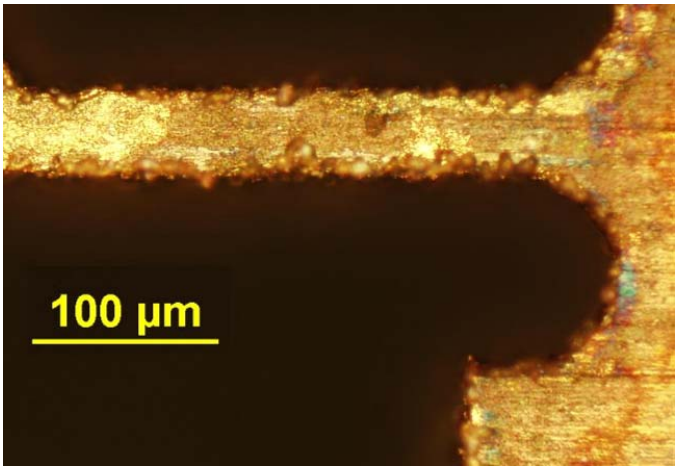

Figure 22

Burrs along edges of a workpiece after μEDM

Assumptions :

1. Model continuous burrs as half of sine wave.
2. Deburr in batch mode that is removing burrs just under the electrode.
3. Deburr one edge at a time.

Consider the case as shown in Figure 23(a) where burrs are modeled as an absolute sine wave of magnitude h and period P. A top view of the burrs along the edge of the workpiece and position of the tool is shown in Figure 23(b).

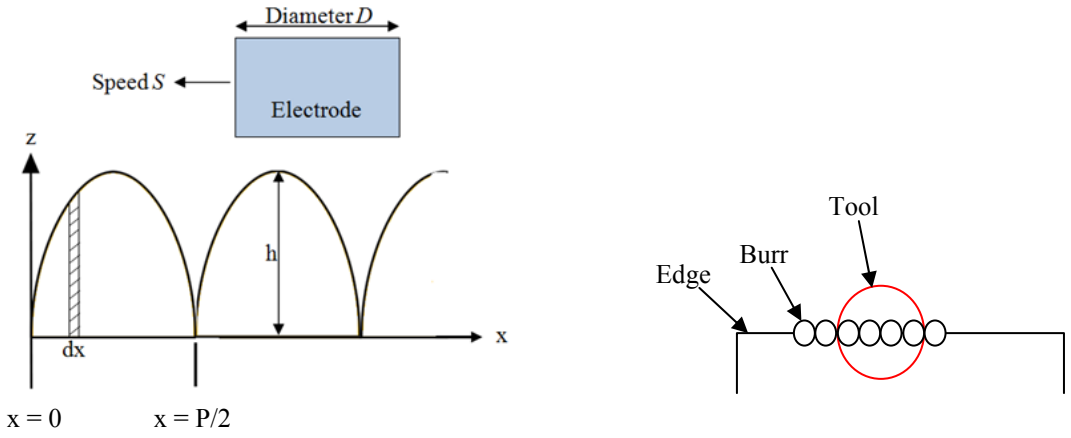

(a) (b)

Figure 23

Burr model and tool position

(a) Modeling of burr formations (b) Top view of edge burr and tool position

The sine wave is of the form,

$$z = \left| h \sin\left(\frac{2\pi x}{\mathrm{P}}\right) \right| \tag{20}$$

The volume of these burrs is obtained by finding the volume of rotation of the sine curve about the x axis. The volume of an infinitesimal segment of thickness dx is given by Equation (21).

$$dV = \frac{\pi z^2 dx}{2} = \frac{\pi h^2}{2} \sin^2\left(\frac{2\pi x}{\mathrm{P}}\right) dx \tag{21}$$

The volume of a single burr V_s between x = 0 and x = P/2 on the surface is obtained by Equation (22).

$$V_s = \frac{\pi h^2}{2} \int_0^{P/2} \sin^2\left(\frac{2\pi x}{P}\right) dx \tag{22}$$

The number of burrs b under the tool is given by Equation (23).

$$b = \frac{D}{P/2} \tag{23}$$

The volume of burrs removed by the tool at any position is given as $V_s.b$

The volume of burrs over a length l of the sample is given by Equation (24).

$$V_l = b.\frac{l}{D}.\frac{\pi h^2}{2} \int_0^{P/2} \sin^2\left(\frac{2\pi x}{P}\right) dx \tag{24}$$

where V_l is the total volume of burrs along the edge length l.

Recall that the volume of material removed per pulse V_u was given by Equation (15).

$$V_u = \int_0^{\tau} \frac{CEAdt}{gr}$$

The number of pulses required to remove the volume V_l is given by Equation (25).

$$N = \frac{V_l}{V_u} = \frac{b.\frac{l}{D}\frac{\pi h^2}{2}\int_0^{P/2}\sin^2\left(\frac{2\pi x}{P}\right)dx}{\int_0^{\tau}\frac{CEAdt}{gr}}$$

$$= \frac{b.\frac{l}{D}\frac{\pi h^2}{2}.\frac{P}{4}}{\int_0^{\tau}\frac{CEAdt}{gr}} \tag{25}$$

In the case where C, E, A, g and r are constants, Equation (25) simplifies to the form,

$$N = \frac{bl\pi h^2 P}{8D\left(\frac{CEA}{gr}\int_0^{\tau}dt\right)} = \frac{bl\pi h^2 Pgr}{8DCEA\tau} \tag{26}$$

The number of pulses N can be represented in terms of time based on pulse duration. If the pulse duration is τ, then the time required is N* τ. Since the length l of the sample to be deburred is known, the speed S at which the tool needed to traverse the surface is calculated using Equation (27).

$$S = \frac{l}{N\tau} \tag{27}$$

The number of pulses as obtained from Equation (26) and the speed obtained from Equation (27) were used to program the stepper motor accordingly using COSMOS software.

4. SYSTEM DESIGN

4.1. SETUP

The µECM system that was developed consisted of many components. A schematic of the various system components is given in Figure 24.

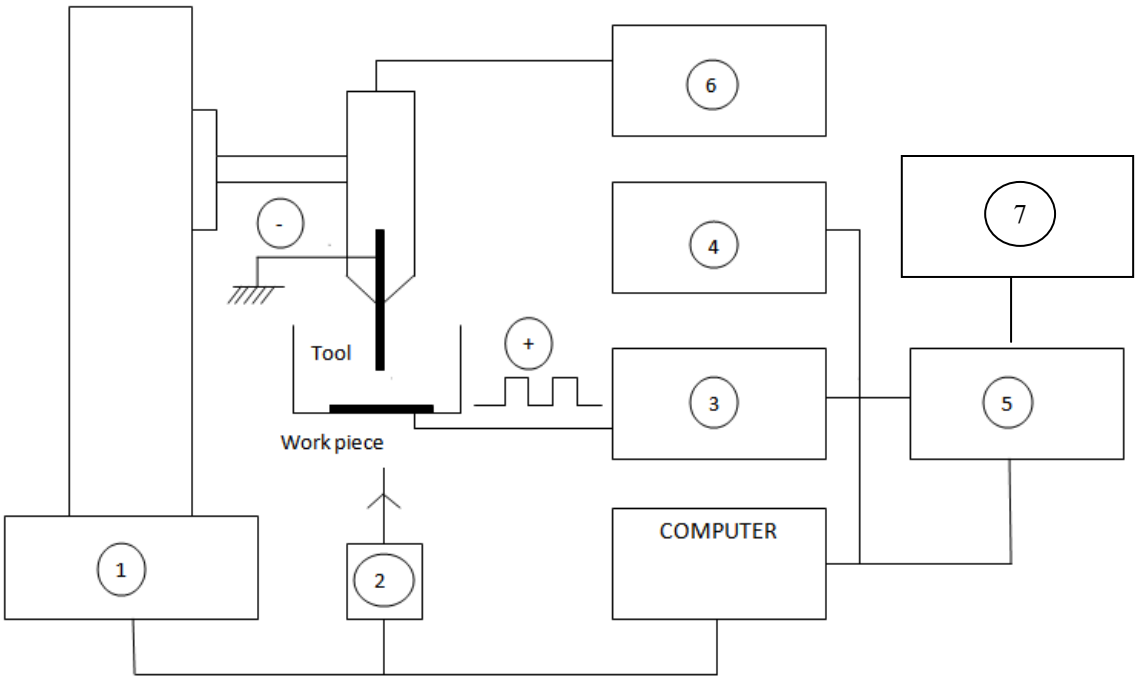

Figure 24

Schematic of the µECM setup

The system components are listed below,

1. Velmex Bi-Slide and VXM-1 controller.
2. Keyence LK-G157 laser head and LK-G-3001V controller.
3. Agilent 33250A function generator.
4. Tektronix TDS 1002B oscilloscope.
5. Fluke 45 multimeter.
6. Conair electrolyte pump.
7. Pioneer XR-P310 amplifier.

4.2. DESCRIPTION OF COMPONENTS

4.2.1. Velmex Bi-Slide and VXM-1 Controller

The Velmex Bi-Slide is a modular system of positioning stages and hardware that allows to quickly and easily creating a complete multi-axis, high accuracy positioning system with lead screw resolution of 0.00025", and repeatability of 0.00015".[1] The Bi-Slide is designed to accommodate NEMA size 23 and 34 motors which can be used for precise positioning applications. The Bi-Slide can be controlled by a computer by means of suitable interface.

[1] www.bislide.com

The major advantages of Bi-Slide are:

- Higher strength to weight ratio – uses hard aluminum alloys and a strong I-beam cross section.
- PTFE bearings deliver much lower friction than metal sliding on metal.
- Operates without lubricant.
- Resistant to impact loads.
- 300 lb load carrying capacity.

The use of this positioning system enabled the tool movement to be controlled by a computer and the system could be automated.

Micro tool movement within the micro machining zone was highly crucial for effective machining to take place (Bhattacharyya, Malapati, and Munda 2005).The Bi-Slide that was configured for use with this system can move in the X and Z axis and rotate about the X axis. The tool was mounted on an arm that was securely fastened to the Bi-Slide a shown in the Figure 25.

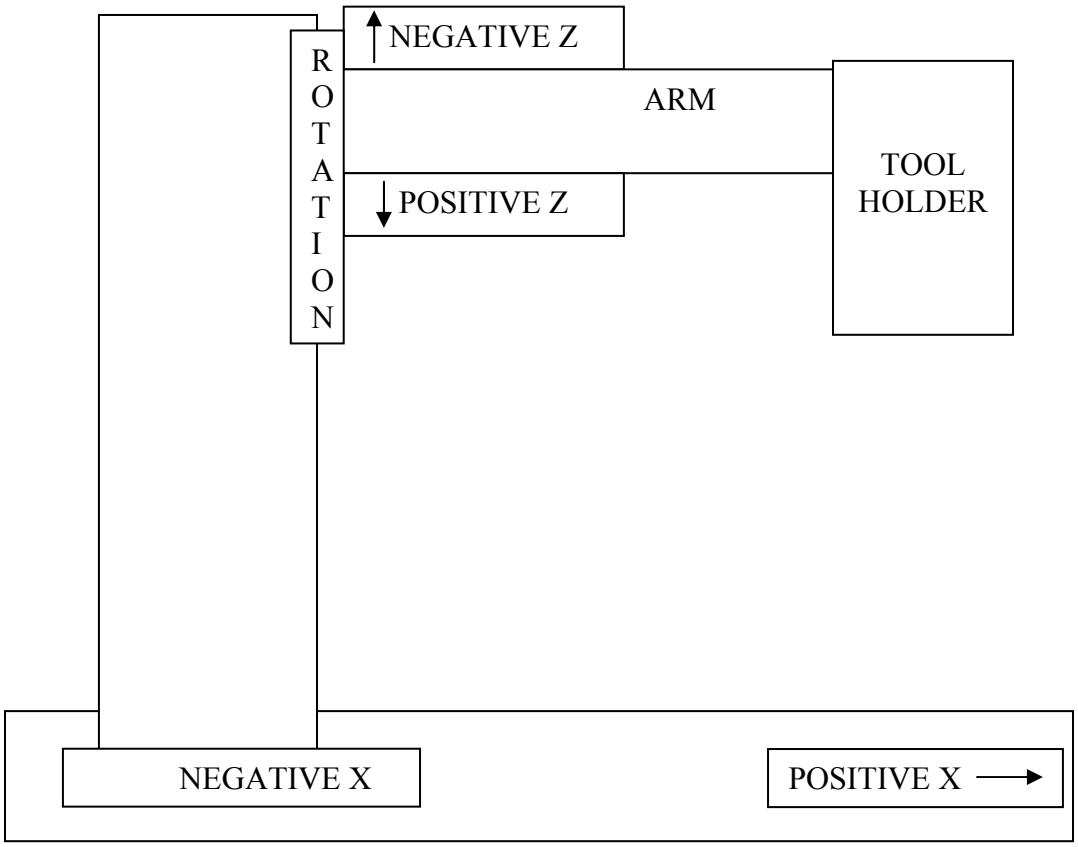

Figure 25

Schematic of Bi-Slide with arm

The stepper motors are controlled by COSMOS software. Stepper motors move the desired distance either in the forward or reverse direction depending on the number of pulses received by them and the sequence in which they are received. The stepper motors can be programmed to move the desired distance in a particular direction with a suitable delay between the pulses so that a wide variety of profiles can be machined. Manual operation of the stepper motors is also possible with the aid of the controller

provided. The software also provides the capability of stopping the motor at any instant of time in case of emergency.

4.2.2. Keyence LK-G157 Laser Head and LK-G3001V Controller

This laser system is a 2 dimensional measurement sensor that was used in conjunction with the Bi-Slide to precisely the position the tool with respect to the workpiece. The main features of this measurement sensor are:

- Sampling speed of 50 KHz
- Accuracy of ±0.5% and resolution of 0.5μm[2].
- Capable of accurately measuring targets rotating or vibrating at high speed.
- Incorporates state of the art algorithms for measuring plastic, transparent or translucent, and metal targets effectively.
- Optimal setting of head and data gathering from controller though computer by provided software.

The provided software LK-Navigator enables the user to optimize the laser beam to effectively measure the surface being measured. The measurement sensor was used to position the electrode in close proximity to the workpiece which is in the order of a few microns and to measure the distance traversed by the electrode.

---

[2] www.keyence.com

4.2.3. Agilent 33250A Function Generator

The Agilent 33220A produces 11 standard wave forms in the frequency range from 0.2 KHz to 80 MHz. The knob or numeric keypad can be used to adjust frequency, amplitude, offset, and other parameters. Internal AM, FM, PM, FSK, and PWM modulation make it easy to modulate the waveforms without the need for a separate source.

4.2.4. Tektronix TDS 1002B Oscilloscope

This oscilloscope has a bandwidth of 60 MHz and a sampling rate of 1 GS/s. The oscilloscope was used to analyze the pulsed power supply and the change in pulse parameters during machining.

4.2.5. Pioneer XR-P310 Amplifier

The amplifier was used to boost the output voltage from the function generator. Higher machining voltages would increase the material removal rate and decrease the machining time.

4.2.6. Conair Electrolyte Pump

The pump was used to circulate the electrolyte in the system. The flow rate could be varied by changing the setting on the pump. The pump dispenses electrolyte in the form of pulses that effectively flush the reaction products from the machining zone.

4.2.7. Fluke 45 Multimeter

The multimeter was used to measure the current in the machining zone. The current in the machining zone is an indication of the gap and can be used as a means of monitoring the gap.

The system design was performed in such a way that the effect of various parameters could be studied. The design of system included design of tool (cathode), workpiece fixtures so that the desired end results of micro machining were achieved. There are a number of constraints that need to be considered for this design because the system needs to machine micro scale components:

- High rigidity.
- Corrosion resistance.
- High precision.
- Minimum electrical resistance.
- Effective ion flushing.
- Environmentally friendly.
- Cost effective.
- Can be implemented for mass production.

The effect of these constraints on the design and the degree to which they are important are discussed below:

High Rigidity: The whole system needs to be highly rigid as the system is being used at micro scale. The system consists of hardware like pump for circulating electrolyte, slides with stepper motor control for moving tool, and other electronic equipment. All these equipment need to be positioned on work table. The pump induces vibration into the whole setup because of the motor. The slide on which the tool is to be mounted needs to be rigidly mounted as otherwise the tool would vibrate and expected results are not obtained. The system was setup

on granite block so that all the vibrations generated by the pump and environmental conditions are absorbed by the block.

Corrosion resistance: The materials that are used in the tool, workpiece fixtures, and other electrical connectors should be corrosion resistant. The electrolyte is a salt solution and it has a tendency to corrode material. The selection of materials needs to be performed carefully so that they are corrosion resistant to obtain the desired results and avoid the problem of frequent replacement of tool, tool holder, and other fixtures. The tool holder was made out of Stainless Steel with some plastic parts in it. The tank was made entirely of plastic to eliminate the problem of corrosion. The electrical connectors were also made of stainless steel.

High precision: This is the most important constraint that needs to be considered because of the scale at which the system is expected to operate under ideal conditions. The stepper motor needs to be highly precise as it is used to move the slide and position the tool at the desired height with respect to the workpiece. Any other positioning system that is being used in conjunction with the stepper motor control needs to be highly precise. The positioning of the tool has to be precise with respect to the workpiece as the gap between them is in the order of a few μms. The stepper motor and the laser system used in conjunction with the stepper motor have repeatability in micron range.

Minimum electrical resistance: The tool and workpiece are connected to the power supply by means of electrical connectors. There is eventually a loss of some power at these connections resulting in the power being supplied not being

used fully for machining resulting in undesirable results. There is power loss not only at these connections but also at interfaces of tool and workpiece with rest of the system. These interfaces need to be properly coated with a layer of insulating material so that there is no power loss at them. The connections among the various electronic equipment were minimized so that there is no loss of power due to resistance. The fixture on which the workpiece was mounted was also made of non conducting material so that resistance offered by it was eliminated.

Effective ion flushing: The tool is in close proximity to the workpiece in μECM and the reaction products at the electrodes need to be flushed away from the small gap between the tool and electrode. Inefficient flushing would impede further machining as the reaction products would short the circuit. This results in the need for an efficient flushing mechanism which can be accomplished by a pump that can both pump and recirculate the electrolyte with suitable filtering mechanism. The electrolyte was being pumped by a pump at high speed that flushed away the reaction products from the gap .The tool holder was designed in such a way that it streamlined the electrolyte flow around the electrolyte aiding in the flushing.

Environmentally friendly: The electrolyte needs to be chosen in such a way that it is free of any toxic component because of disposal problems. The addition of some kind of acid has proved to be effective in reducing the machining time (Bhattacharyya,Malapati, and Munda 2005) but at the same time involves problems associated with its usage.

Cost effective and suitable for mass production: The process also needs to be suitable for mass production as otherwise industries would not find it lucrative enough. The whole setup is such that it can be easily automated.

4.3. DESIGN OF TOOL HOLDER

The tool shape is normally an inverse or negative image of the profile desired in the workpiece. There is no proven technique for determining the exact shape of the tool. The main criteria that were considered in the design of tool holder were:

- Compact in size.
- Corrosion resistance.
- Capable of accommodating a large range of electrodes.
- Streamlining the electrolyte flow.

After a thorough analysis of these factors the design for tool holder was made as shown in Figure 26.

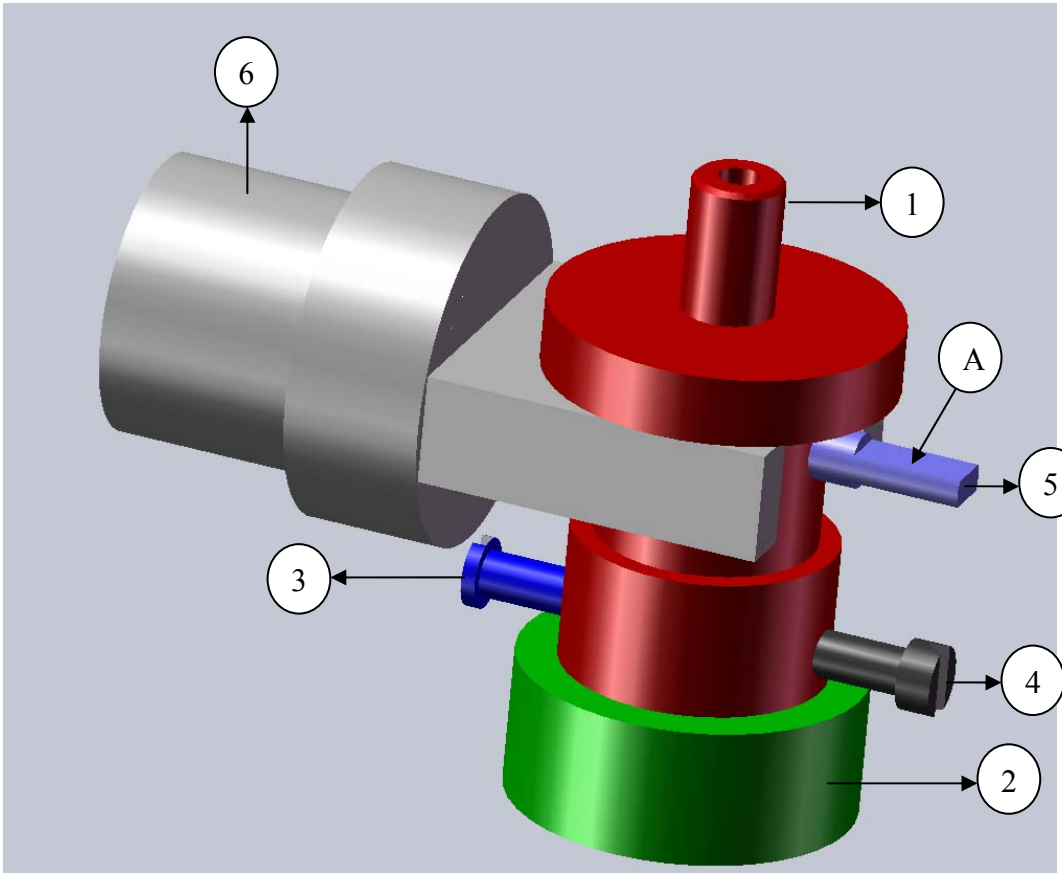

Figure 26

Isometric view of tool holder

Item “1” is the main body of the tool holder in which the electrode is positioned by means of screws “3” and “4”. The ends of screws “3” and “4” are machined to achieve the clamping of electrode. Item “2” is used to streamline the electrolyte. Item “5” is a dowel pin whose end is ground flat and press fit onto the workpiece. The laser is shined onto the flat surface “A” of the dowel pin for measuring the gap as shown in Figure 25. Item “6” is the arm that is connected to the Bi-Slide with the tool holder assembly mounted on it.

4.4. DESIGN OF ELECTROLYTE BATH

The electrolyte bath design was done such that it is simple when considered from the machining angle but at the same time has all the aspects that a cell for micro machining is supposed to possess. The design as shown in Figure 28 was proposed for the cell for μECM. Item "A" is the flat plate with leveling screws on which the assembly is mounted. Item "B" is the tank for holding the electrolyte. Item "C" is a PVC plastic pipe on which the workpiece fixture is mounted. Item "D" is a hose connecting electrolyte tank to pump. The workpiece fixture is a PVC plastic pipe ("E") with a flat face which can be used with a variety of clamps ("F") to accommodate wide range of workpiece sizes as shown in Figure 27.The cross sectioned view of workpiece fixture is shown in Figure 29.

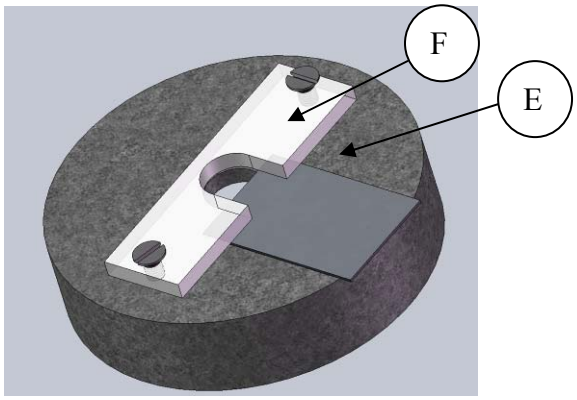

Figure 27

Workpiece fixture

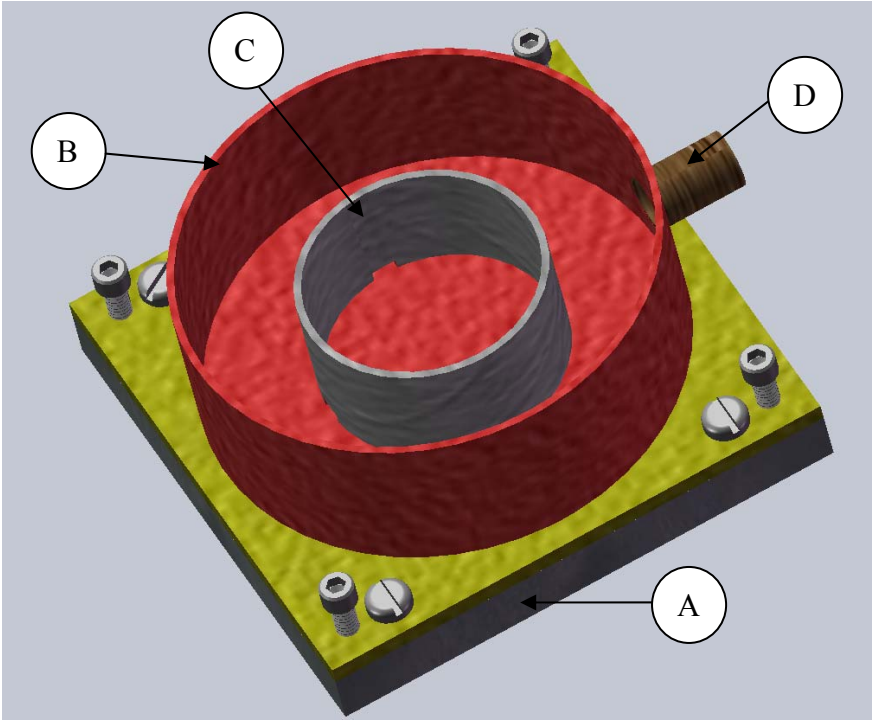

Figure 28

Solid model of electrolyte bath

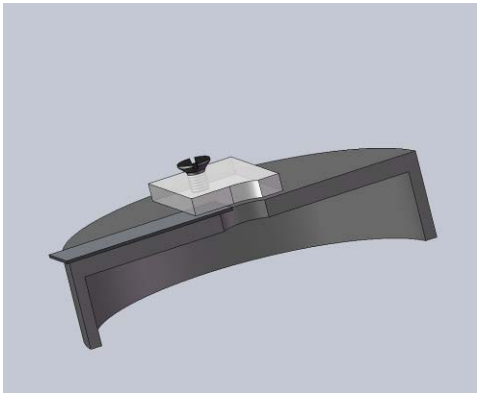

Figure 29

Cross sectioned view of workpiece fixture

4.5. TOOL SETUP

The electrode used in the experiments was made of stainless steel. The electrode was positioned in the tool holder and secured in place by the specially shaped fasteners from the sides. The length of the electrode protruding out of the tool holder was measured by means of an optical microscope. The tool holder with the electrode in place was positioned on the flat plate and mounted on the arm of Bi-Slide.

4.6. WORKPIECE SETUP

The workpiece specimens were 30 mm x 20 mm x 100 μm sheets. The workpieces were thoroughly cleaned ultra sonically before machining. The workpiece was rigidly held in position by using an appropriate clamp. The fixture containing the workpiece was mounted onto base and the flatness of the workpiece surface ensured by the laser measurement sensor. The laser sensor was used to measure the distance at various locations on the workpiece and the leveling screws were adjusted to ensure the workpiece was flat.

4.7. TOOL POSITIONING

The laser sensor was used to measure the distance from the workpiece surface to laser head. The laser sensor was zeroed on the surface of workpiece that means the sensor gave the reading as zero when focused on the surface of workpiece. The sensor was then used to measure the distance from the flat surface of the dowel pin. The method that was adopted for measuring the gap is depicted in Figure 30.

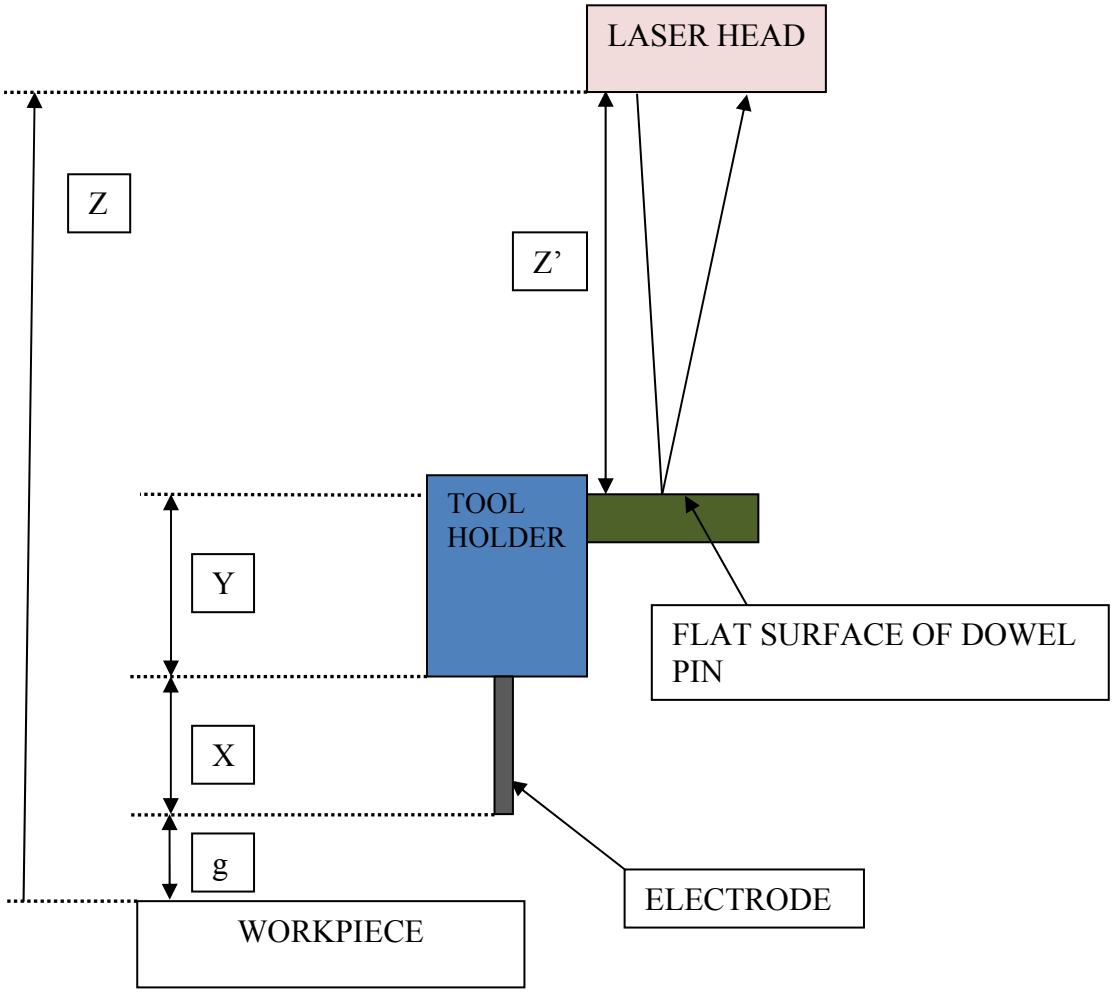

Figure 30

Schematic showing gap measuring technique

Procedure:

1. The length X was measured using microscope.

2. Y was already known from design.

3. Z' was the reading given by the laser sensor when focused on flat surface pf dowel pin.

4. The gap between the electrode and the workpiece (g) is given as,

$$g = Z - (X + Y + Z')$$

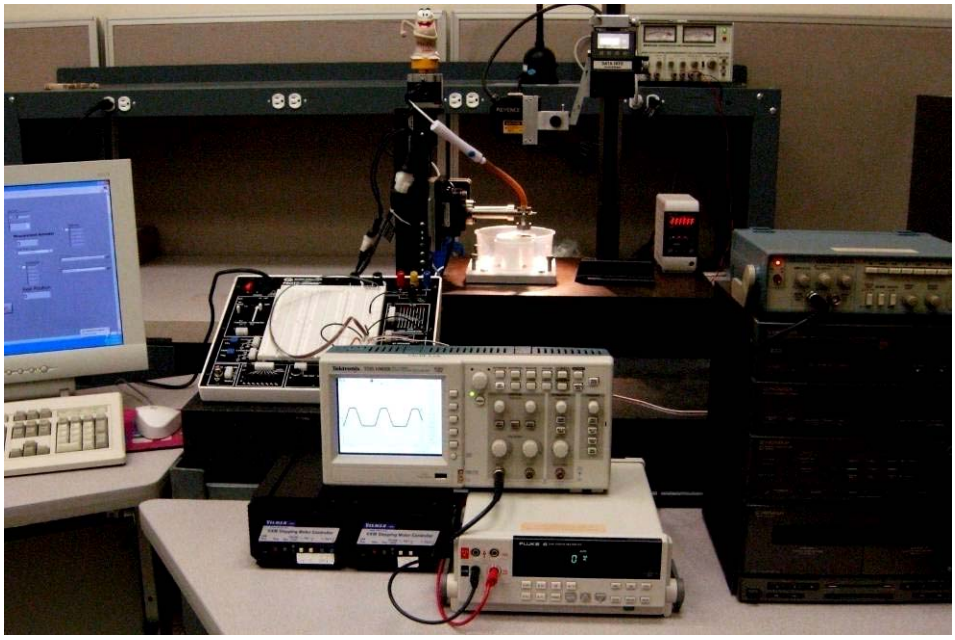

Figure 31

The μECM system

The complete μECM system is shown in Figure 31. A semi automated process was developed to drill small holes on a workpiece. The program for controlling the

stepper motor was developed such that the tool progressed slowly into the workpiece to the desired depth beginning at a height of 100μm from the workpiece surface and retracted back to a higher level. The stepper motor moved the tool by a distance of 2.5 μm for every step. There was a delay between steps for machining to take place. The program for deburring was developed such that the tool maintained a constant gap as it traversed across the surface of the workpiece.

The tool was brought to the desired height from the work surface with the aid of the laser sensor. The pump and the power supply were turned on at the same time. COSMOS software was used to transmit the pulses to the stepper motor and the electrode progressed into the workpiece starting machining. The voltage and the current were noted down periodically from the oscilloscope and the multimeter respectively as machining progressed.

4.8. CLOSED LOOP VS OPEN LOOP OPERATIONS

A feedback loop based on current was designed using LabVIEW. The current in the machining zone was monitored and if the current went above a preset limit the electrode was retracted to a higher level bringing the machining to a halt. The reason for this being that machining could take place only if the tool and workpiece were in close proximity.

The interface developed requires the hole depth to be drilled, the delay between the stepper motor pulses and the upper limit of current value as input.

5. EXPERIMENTS

A number of experiments were carried out to study the characteristics of the system. All results were obtained by open loop experiments unless specified.

5.1. PROCESS PARAMETERS

The parameters ranges for the experiments are tabulated in Table 4.

Table 4

Parameter range

Electrode	Stainless steel
Workpiece	Copper alloy (CA-173), Stainless steel (SS-316L)
Electrolyte	3 % Sodium nitrate ($NaNO_3$)
Frequency	0.5 KHz to 50 KHz
Voltage	16 Vpp - 24 Vpp
Delay between pulses	0.1 sec to 5 sec

The function generator provided DC pulsed power supply with a peak to peak voltage of 16 V. The frequency selected for experiments ranged from 0.5 KHz to 50 KHz. The oscilloscope was used to analyze the output of the function generator and aided in setting the function generator to the desired voltage and frequency. The electrolyte used was freshly prepared 3 % sodium nitrate ($NaNO_3$) solution.

5.2. DRILLING OF COPPER

This set of experiments aimed to drill holes in CA-173 workpiece and study the condition of electrodes after machining, entrance and exit profiles of drilled holes and the effect of frequency on MRR.

The electrode used in these experiments was a Ø660 µm SS-316L unless otherwise specified. The end was ground using 400 grit sand paper and then polished using 1 µm alumina particles. A groove was machined on the electrode by Electric Discharge Machining. The workpiece was 30 mm x 20 mm x 100 µm CA-173 sheet. The electrolyte was 3% $NaNO_3$ solution.

A total of 10 electrodes were prepared and numbered 1 to 10 using a diamond marker to study the electrode condition. The electrode was a Ø500 µm stainless steel pin whose end was ground flat and polished. The number of holes drilled with each electrode was equivalent to the number with which it was marked. All the holes were drilled at 16 Vpp and 0.5 KHz. The program named "CA-173-40µm-2sec" (Appendix C) was used with COSMOS which was programmed to drill holes 40µm deep.

Scanning Electron Microscopy Analysis was performed on the electrodes using JEOL JSM-400 Scanning Electron Microscope (SEM) to thoroughly study the deposition on the electrodes. The drilled holes on CA-173 were also studied. Energy dispersive X-ray spectroscopy (EDS) was used with the electrode to study the deposited elements.

The parameters for the experiments in which through holes were drilled are tabulated in Table 5. A total of 2 holes were drilled for each parameter. The program

named “CA-173-Through-2sec” (Appendix C) was used with COSMOS.

Table 5

Parameters for drilling through holes on CA-173 sheets

FREQUENCY (KHz)	0.5, 25
VOLTAGE (V)	16 Vpp (-4 V to 12 V)
DELAY BETWEEN PULSES (seconds)	1.5 sec for 0.5 KHz, 4 sec for 25 KHz
DUTY CYCLE	100% for 0.5 KHz, 66.67% for 25 KHz

The negative voltage was introduced so that there was no deposition on the tool as during the negative polarity cycle material was removed from the electrode. The negative polarity cycle was kept to a minimum so that the electrode did not wear out after a limited number of cycles. The negative polarity gave the electrolyte additional time to flush away the products.

The parameters for the experiment to study the effect of frequency on material removal rate are tabulated in Table 6. A total of 2 holes were drilled for all parameters. The program named “CA-173-40µm-2sec” (Appendix C) was used with COSMOS.

Table 6

Parameters for analyzing effect of frequency on MRR for CA-173 workpiece

FREQUENCY (KHz)	0.5, 1, 3 5, 10, 50.
VOLTAGE (V)	16 Vpp (-4 V to 12 V)
FLOW RATE OF ELECTROLYTE (l/min)	0.31

A map was made with the position of the various holes to identify them while observing them under microscope. The hole diameters and depths were measured using Olympus STM 6 microscope and tabulated. A fixture was made to ensure that the workpiece was flat when viewing under the micro scope. Figure 32 shows the fixture.

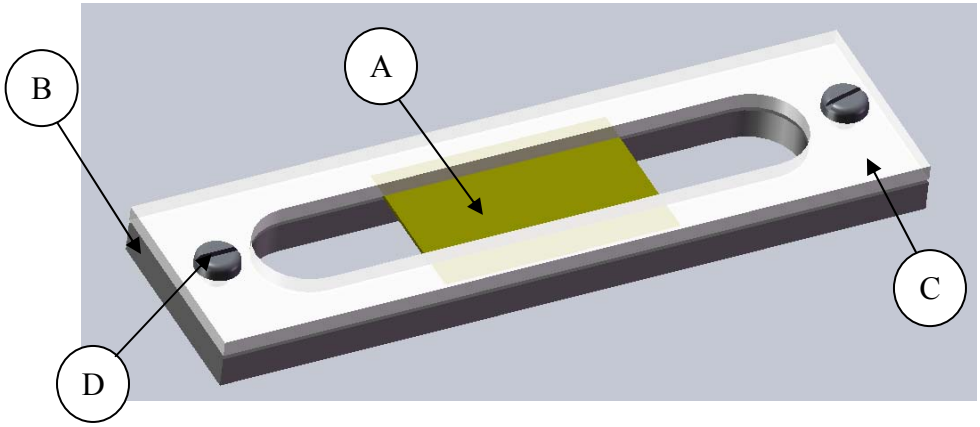

Figure 32

Fixture for viewing workpieces under microscope

The workpiece “A” was clamped in between “B” and “C” which were made of plastic by means of screws “D”.

5.3. DRILLING OF STAINLESS STEEL

This set of experiments aimed to drill holes in SS-316L workpiece and study the effect of frequency on MRR, effect of voltage on MRR and effect of sacrificial layer on hole profile.

The electrode used in these experiments was a Ø660 µm SS-316L. The end was ground using 400 grit sand paper and then polished using 1 µm alumina particles. A groove was machined on the electrode by Electric Discharge Machining. The workpiece was 30 mm x 20 mm x 500 µm SS-316L sheet.

The parameters for the experiment to study the effect of frequency on material removal rate are tabulated in Table 7. A total of 2 holes were drilled for all parameters. The program named "SS-316L-100µm-2sec" (Appendix C) was used with COSMOS.

Table 7

Parameters for analyzing the effect of frequency on MRR for SS-316L workpiece

FREQUENCY (KHz)	0.5, 1, 3 5, 10, 50.
VOLTAGE (V)	16 V pp (-4 V to 12 V)
FLOW RATE OF ELECTROLYTE (l/min)	0.31

The parameters for the experiment to study the effect of voltage on MRR are given in Table 8. This experiment was performed under closed loop condition where the current in the machining zone was used as a feedback signal.

Table 8

Parameters for analyzing effect of voltage on MRR for SS-316L workpiece

FREQUENCY (KHz)	0.5, 10, 50
VOLTAGE (V)	16 Vpp, 24 Vpp
FLOW RATE OF ELECTROLYTE (l/min)	0.31

The experimental procedure and techniques used for experiments in which a sacrificial layer was used are described below:

1. 20 mm x 20 mm x 500 μm SS-316L pieces were cut and deburred with fine sand paper. It was ensured that the pieces were flat. A chamfer was made on the edges of half of the workpieces for differentiation purposes. Figure 33 shows the workpieces with and without chamfer. Numbers were engraved on the workpiece in a sequential manner.
2. 20 mm x 20 mm x 25 μm SS-316L sacrificial layers were cut.
3. A new 660 μm diameter SS-316L electrode was prepared.
4. A total of eight holes were machined on each workpiece. The positioning of the holes on the workpiece is shown in Figure 34.

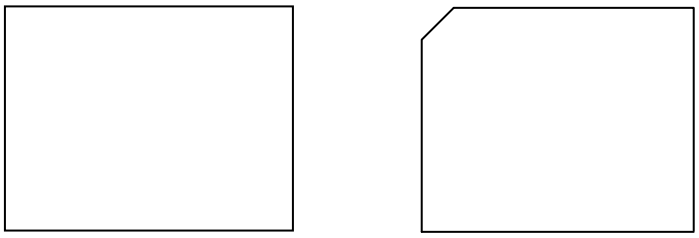

Figure 33

Schematic of workpieces without and with chamfer

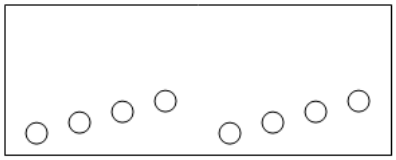

Figure 34

Schematic showing position of holes on workpiece

The positioning of holes was done in this manner to get good results when grinding. The probability of stopping the grinding at the center of hole was very low and hence four holes were drilled to increase the chances.

An amplifier was used to boost the voltage to study the effect of varying the voltage on MRR. A total of 4 workpieces were machined, each having 8 holes. A total of 4 holes were drilled for each set of parameters. The set of experiments were performed with closed loop conditions where the system would monitor the current value and machine accordingly. The parameters for each workpiece are tabulated in Table 9.

Table 9

Parameters for analyzing effect of sacrificial layer

With sacrificial layer				With – out sacrificial layer			
Workpiece I		**Workpiece II**		**Workpiece III**		**Workpiece IV**	
Voltage: 16 Vpp	Frequency: 0.5 KHz	Voltage: 16 Vpp	Frequency: 50 KHz	Voltage: 16 Vpp	Frequency: 0.5 KHz	Voltage: 16 Vpp	Frequency: 50 KHz
Voltage: 24 Vpp	Frequency: 0.5 KHz	Voltage: 24 Vpp	Frequency: 50 KHz	Voltage: 24 Vpp	Frequency: 0.5 KHz	Voltage: 24 Vpp	Frequency: 50 KHz
Chamfer : No		Chamfer : Yes		Chamfer : No		Chamfer: Yes	

After machining, the workpieces were cleaned with an acid solution to clean the oxide layers on the surface that were formed during machining. The acid solution that was used was a mixture of 5 ml nitric acid, 10 ml hydrochloric acid and 15 ml water (ASM Metals Handbook 1973).

Procedure for cross sectioning:

1. The workpieces were thoroughly cleaned ultrasonically for increased adhesion purposes.
2. Workpieces I and II were glued together by means of a nut in between them and workpieces III and IV were glued together by means of two nuts as shown in Figure 35. This was performed ensuring that the workpieces remained flat by using a suitable clamp.

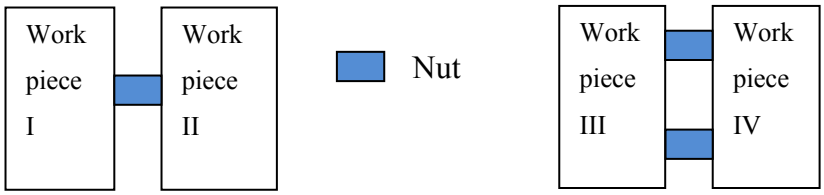

Figure 35

Schematic of workpiece preparation for molding

3. The workpiece pairs were positioned on a silicone tray and the resin prepared. The resin contains an epoxy and a hardener in the right combination. The main constituents of the epoxy and hardener were bisphenol-A and amines respectively. 15 volumes of the epoxy were mixed with 2 volumes of hardener ensuring that no air bubbles were formed. The resin was poured into the silicone tray in which the workpieces were placed and held in vertical position. The resin was poured in such a way that no air bubbles were formed because formation of air bubbles would result in loss of data.
4. The resin was set to cure overnight and the samples were grinded and polished to observe the cross sections. A few of the samples were etched to study the grain structure.

The diameters of the drilled holes were measured at top and bottom in both the X and Y directions. The depths of the holes were also measured. The radius of the round off was measured with Image-Pro Discovery software.

5.4. DEBURRING OF COPPER

This set of experiments aimed at deburring of micro components that were produced by micro Electric Discharge Machining (μEDM). The workpiece that was chosen for this study was a 100 μm thick CA-173 sheet on which micro parts were machined as shown in Figure 36. These micro parts were having burrs on them which were undesirable.

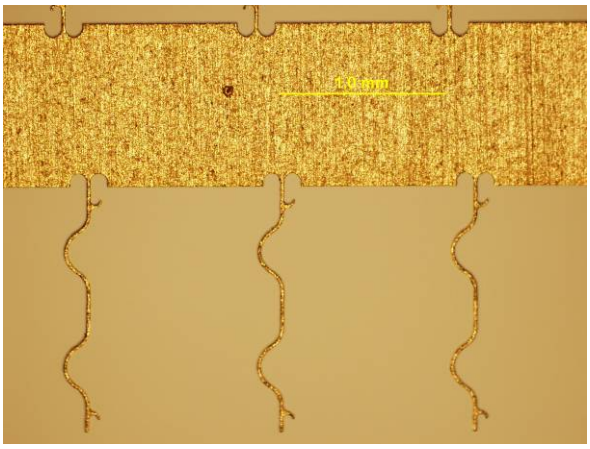

Figure 36

Component machined by μEDM

Procedure:

1. The workpieces were cleaned with an acid solution before machining as they had an oxide layer formed on them. The workpieces were cleaned with 30% sulphuric acid for 15 minutes at 55^{o}C (130^{o}F) and agitated every 5 minutes. They were thoroughly cleaned with water and ultrasonically subsequently.
2. The workpiece was clamped in such a way that the loops were not damaged by the

clamp. A number of experiments were conducted by varying the gap, frequency and the voltage to find the ideal combination of parameters that would deburr effectively. The program named "CA-173-Deburr" (Appendix C) was used with COSMOS.

Table 10 tabulated experimental variables and setup.

Table 10

Parameters for deburring copper

ELECTRODE	Ø500 µm SS-316L
FREQUENCY (KHz)	50
VOLTAGE (V)	16 Vpp (14 V max, -2 V min)
GAP (µm)	100

3. The micro parts were having burrs on both sides and hence the workpiece was turned over and electrochemically machined to deburr the other side. The machined workpiece was cleaned with the acid solution to clean the surface, so that the component could be put to end use.

6. RESULTS AND DISCUSSION

6.1. ANALYSIS OF HOLES DRILLED IN COPPER

Figure 37 shows some kind of layer formed on the surface of CA-173 after machining. It was suspected that this layer impeded machining and further tests were performed to obtain the composition of the layer.

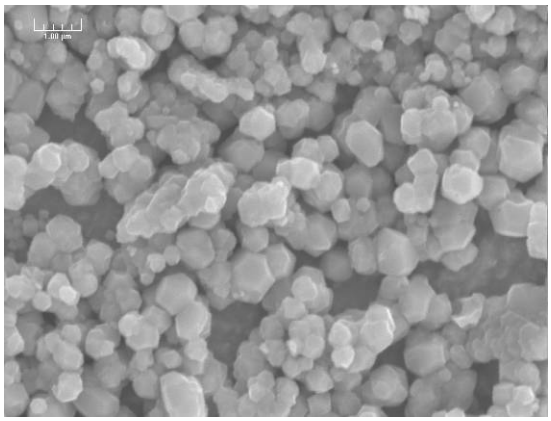

Figure 37

Surface of CA-173 workpiece after μECM at 0.5 KHz and 16 Vpp

Figure 38 shows images of stainless steel electrode that was used to machine 8 holes in CA-173.There was a clear indication of deposition on the electrode. (a) shows the bottom of the electrode whereas (b) shows a side view of the electrode.

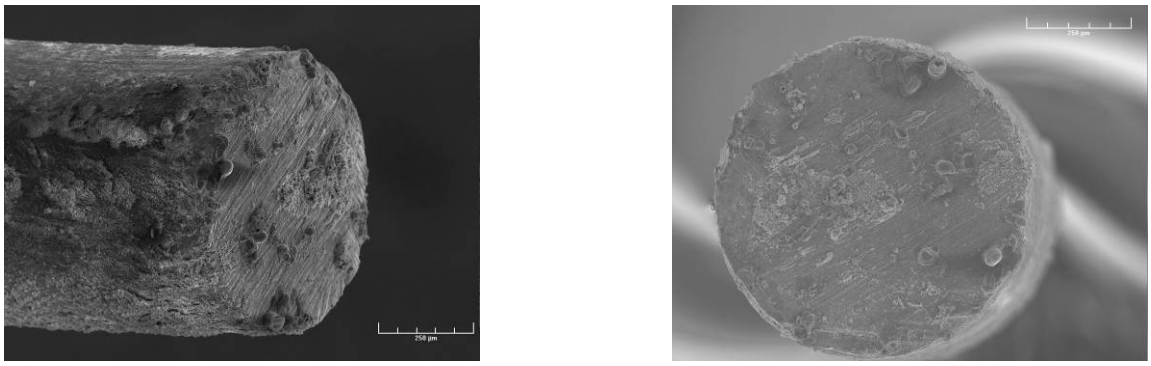

(a) (b)

Figure 38

Stainless steel electrode after machining CA-173 workpiece at 0.5 KHz and 16 Vpp

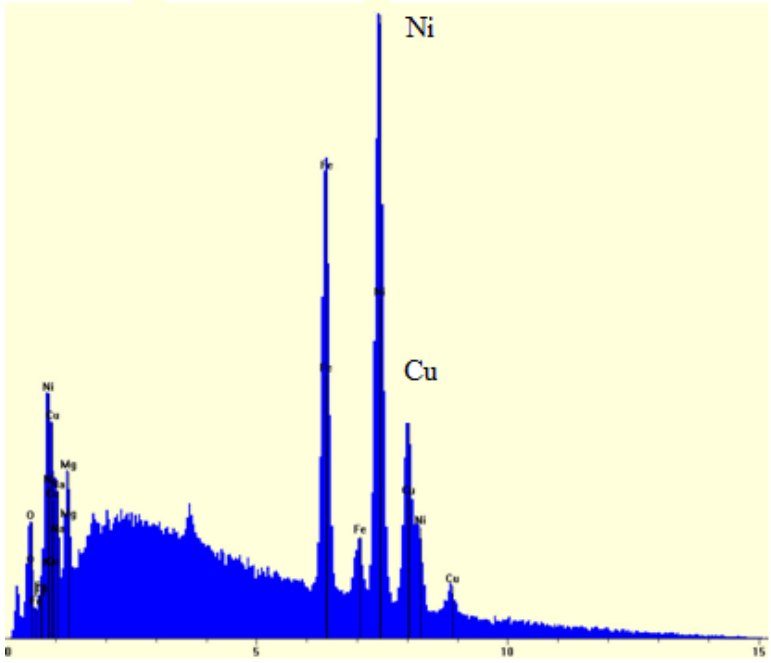

Figure 39

EDS spectrum of electrode after µECM on copper

The plot obtained from EDS on a stainless steel electrode that was used to drill 8 holes in CA-173 is shown in Figure 39. The composition of each element and their source are tabulate din Table 11.

Table 11

Results of quantitative analysis on stainless steel electrode

Element	**Composition (%)**	**Source**
Nickel (Ni)	41.04	Coating on electrode
Iron (Fe)	19.07	Tool material
Copper (Cu)	18.79	Workpiece material
Oxygen (O)	9.42	Oxidation
Sodium (Na)	6.9	Electrolyte

It was observed that there was a high concentration of nickel at the electrode tip. It was found that the commercially available stainless steel pins that were being used as electrodes had nickel coating on them which reacted with the copper and formed a layer of non conductive layer which impeded further machining. This was the reason that the current and voltage readings appeared constant but there was no machining take place.

Figure 40 shows image of a hole drilled on a 100 μm thick CA-173 sheet with a 500 μm diameter stainless steel electrode.

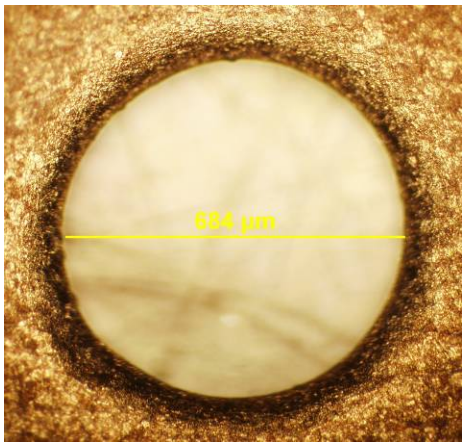

Figure 40

Hole drilled on 100 µm thick CA-173 sheet at 50 KHz and 16 Vpp

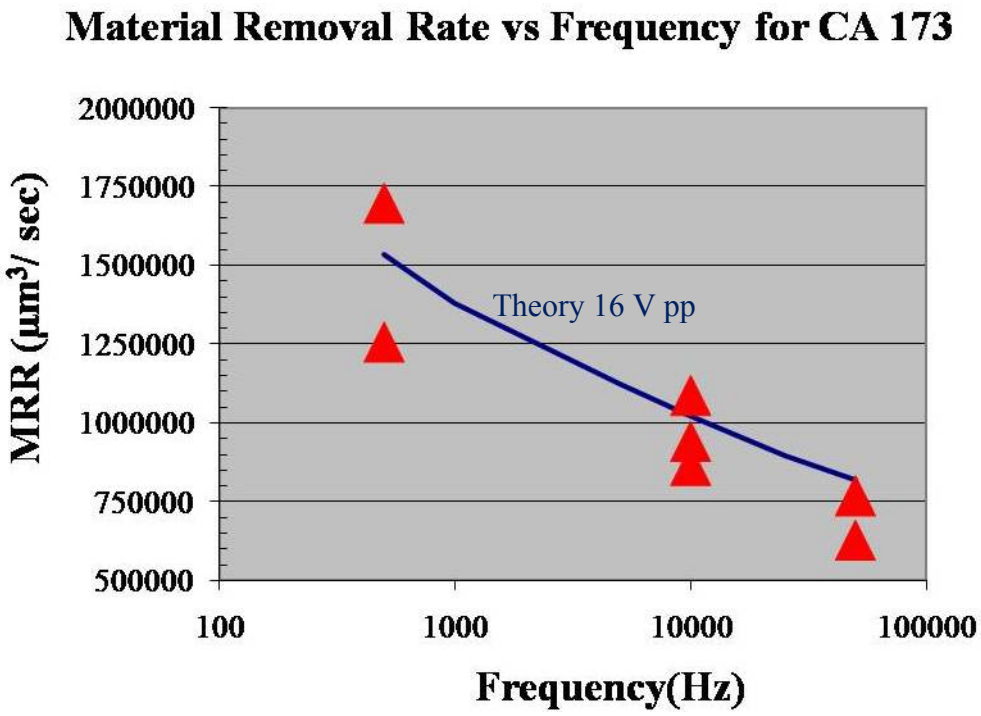

Figure 41

Material removal rate versus frequency for CA-173 with Ø660 µm stainless steel electrode and 16 Vpp

The material removal rate is inversely related to the frequency as given by Equation (16). Figure 41 shows the plot of material removal rate versus frequency for holes machined on CA-173 workpiece.

It was observed that the material removal rate decreased with an increase in frequency. At very high frequencies the material removal rate was very low and the duty cycle needed to be low so that the electrolyte had more time to flush away the reaction products.

The effect of frequency on MRR was shown in Figure 16. It was observed that the MRR increased with increase of pulse ON time which was in accordance with the results obtained as the MRR decreased at higher frequencies.

6.2. ANALYSIS OF HOLES DRILLED IN STAINLESS STEEL

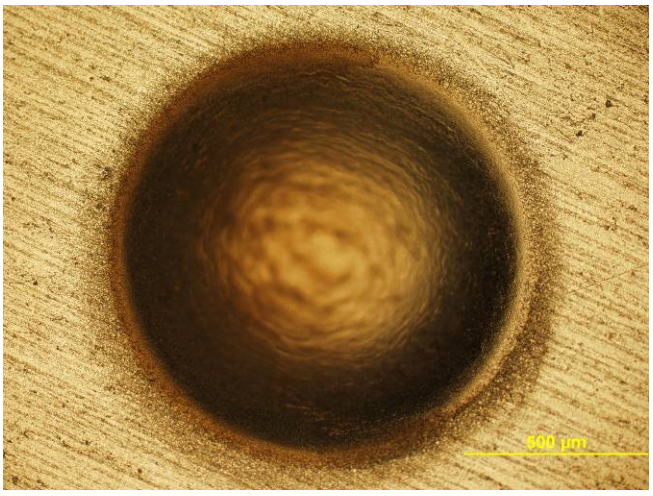

Figure 42

Optical image of hole drilled on 500 µm thick SS-316L sheet at 0.5 KHz and 16 Vpp

Figure 42 shows image of a hole drilled on 500 µm thick SS-316L sheet with a Ø660 µm SS-316L electrode.

It was reported by Viola Kirchner et al. (2001) that the addition of fluoride and chloride ions was crucial for micro machining of stainless steel. As a result of oxidation, passivation layer of iron, chromium and nickel were formed on the surface inhibiting further machining. The addition of the halide ions destabilized the oxide so that further machining could progress. The set of experiments were conducted without the addition of any acid due to the difficulties in handling them and in compliance with lab policies.

Figure 43 shows the top surface of a hole drilled in SS316L. The observation of grain structure indicated that electrochemical machining eroded grain boundaries due to high strain energy at grain boundaries.

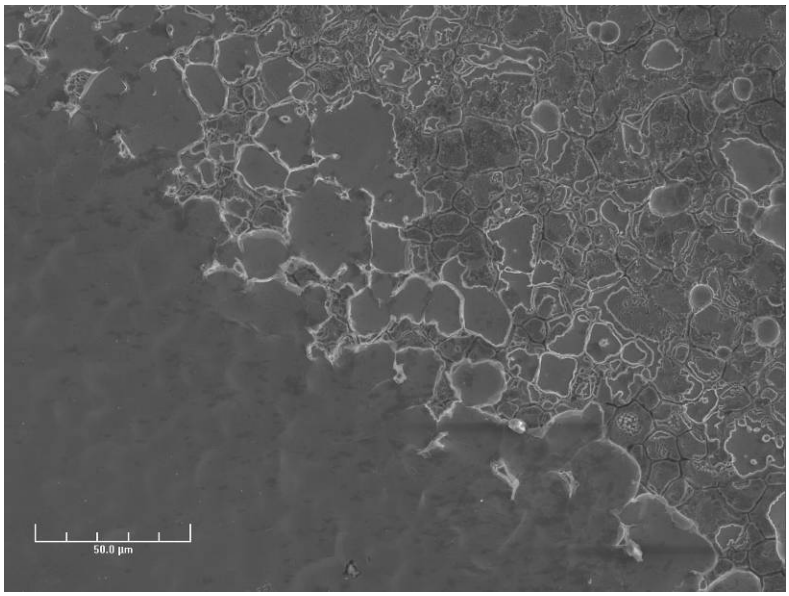

Figure 43

Circumference of hole drilled on SS-316L workpiece at 1 KHz and 16 Vpp

The picture showed differences in texture because in the region where there was electrolyte flow machining tool place and grain structure was visible. Figure 44 shows image of a hole drilled on 500 µm thick SS-316L sheet. It was observed that the edges were smooth without any burrs emphasizing the fact that µECM produces workpieces without any burrs.

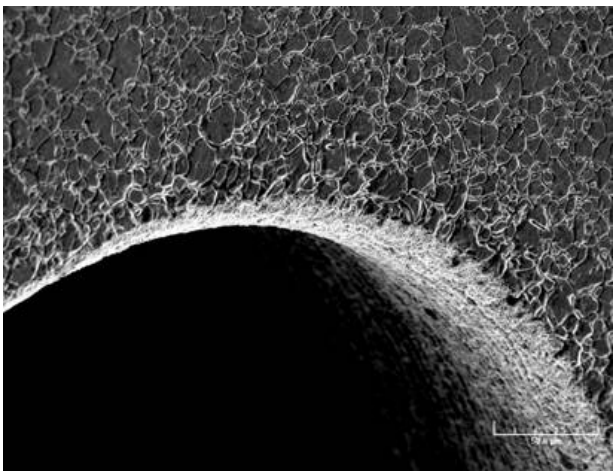

Figure 44

Hole drilled on 500 µm thick SS-316L sheet at 1 KHz and 16 Vpp

Pulsating current has three parameters: pulse on time, pulse off time, and peak current density which can be varied independently to achieve desired machining rate. By suitable choice of the above parameters, variations of electrolyte conductivity in the machining region could be reduced and high, instantaneous mass transport achieved even at low electrolyte flow rates. The appropriate selection of length and duty of pulse was essential to obtain the best surface quality. Experiments performed to study the effect of variation in pulse on time and pulse off time on surface quality indicated that

short pulse on time and high pulse off time yield improved surface with less pitting (Rajurkar et al. 1999).

The experiments that were conducted maintained the same pulse on/off time while machining at low frequencies. The pulse off time was more than the pulse on time at high frequencies to enable the electrolyte to flush away the machining products which was in accordance with existing data. Figure 45 shows plot of surface roughness versus pulse on and pulse off time.

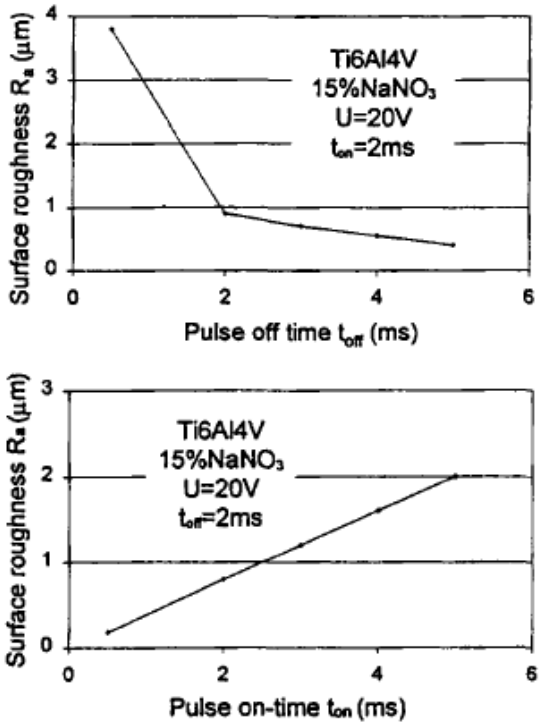

Figure 45

Plot of surface roughness versus pulse ON/OFF time (Rajurkar et. al. 1999)

The material removal rate is directly dependent on the working voltage as given by Equation (15). Figure 46 shows the effect of voltage on material removal rate for holes machined on 500 µm thick SS-316L workpiece.

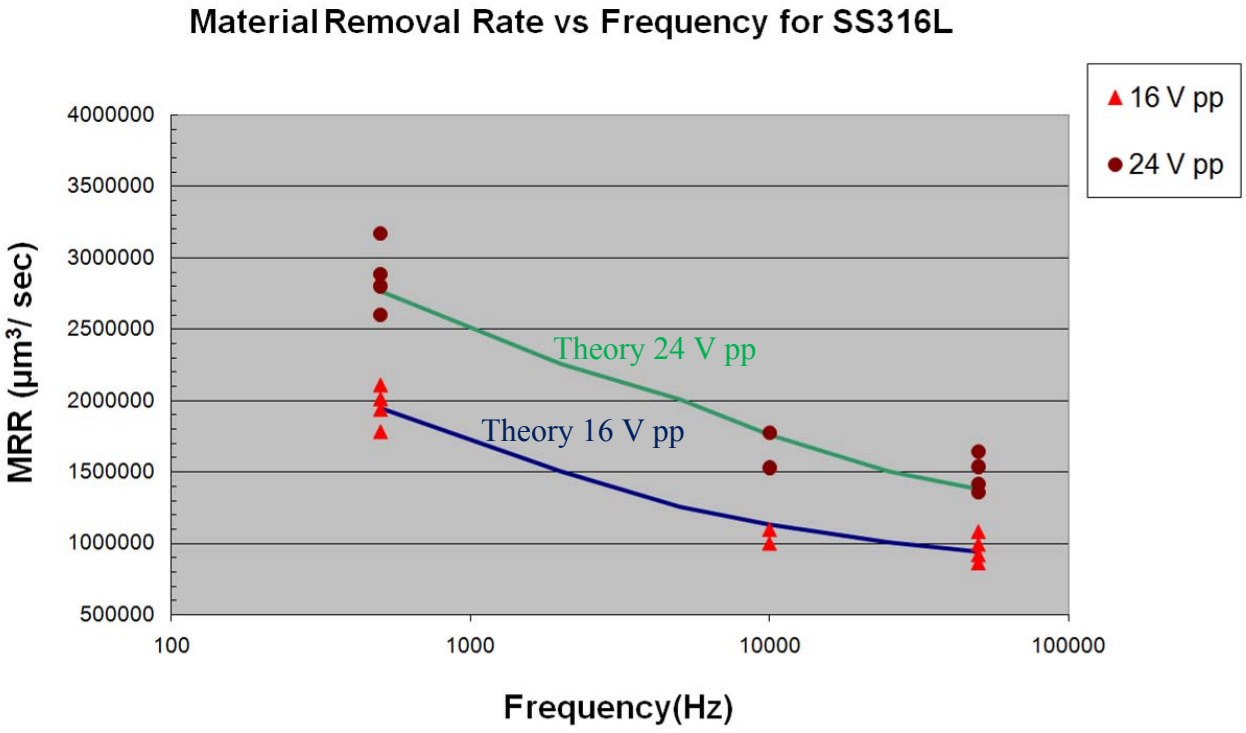

Figure 46

Effect of voltage on material removal rates in closed loop operation on SS-316L workpiece with 3%$NaNO_3$

It was observed that the MRR increased with voltage. The current density in the machining zone increased with increase of voltage and hence the rate at which the anode dissolved increased according to Faraday's laws. The experimental values obtained were in agreement with the developed model except for slight variations which could be

attributed to factors like inefficient electrolyte flushing when the gap became really small.

The effect of voltage on material removal was shown in Figure 15. It was observed the MRR showed an increase with an increase in voltage which was in accordance with the results obtained.

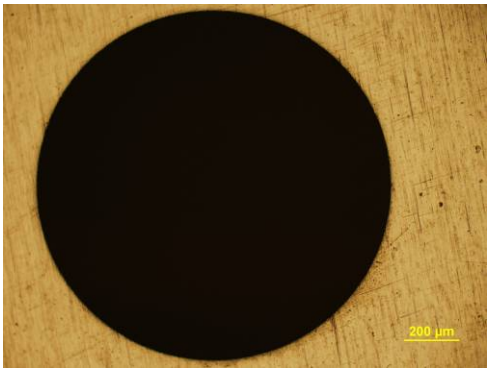

Figure 47

Exit side of hole drilled in 25 µm thick SS-316L sacrificial layer at 50 KHz and 24 Vpp

The presence of sacrificial layer enhanced the hole profile as much of the surface distortion occured on the sacrificial layer rather than the actual workpiece. Figure 47 shows the exit side of hole drilled through a 25 µm thick SS-316L sacrificial layer. Figure 48(a) shows the top surface of a hole that was drilled with a sacrificial layer on top of it.

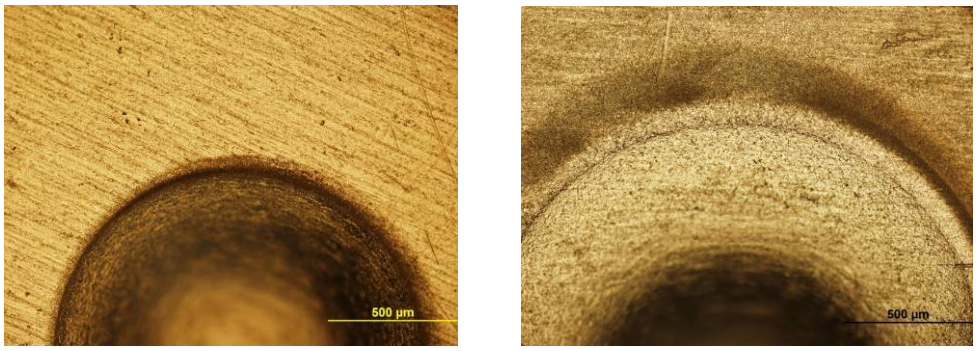

(a) (b)

Figure 48

Comparison of holes drilled with and without sacrificial layer

(a)Entrance of hole drilled in SS-316L with sacrificial layer at 50 KHz and 24 Vpp

(b)Entrance side of hole drilled in SS-316L without sacrificial layer at 50 KHz and 24 Vpp

It was clearly observed that the circumference was straight without any distortions when sacrificial layer was used unlike the hole shown in Figure 48(b) which was machined without sacrificial layer.

The cross sections were analyzed to study the rounding off at lower frequencies and the effect of sacrificial layer on the rounding off. Figure 49 shows the cross section of a hole drilled in 500 µm thick SS-316L workpiece without sacrificial layer.

Figure 50 shows cross section of a hole drilled on 500 µm thick SS-316L workpiece with a sacrificial layer.

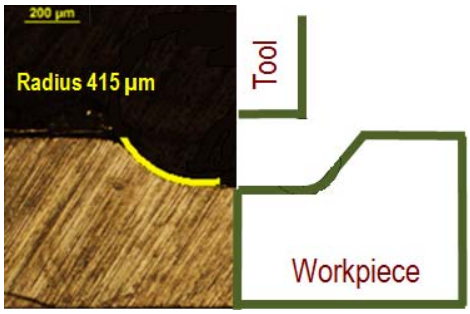

Figure 49

Cross section of hole drilled in SS-316L without sacrificial layer at 50 KHz and 16 Vpp

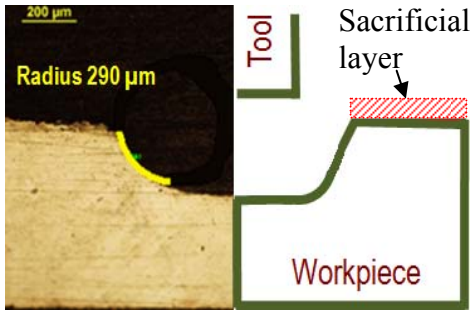

Figure 50

Cross section of a hole drilled in SS-316L with sacrificial layer at 50 KHz and 16 Vpp

Figures 49 and 50 clearly demonstrate the improvements obtained with the sacrificial layer. The round off radius was 415 µm for the hole without sacrificial layer where as for the hole with sacrificial layer it was 290 µm.

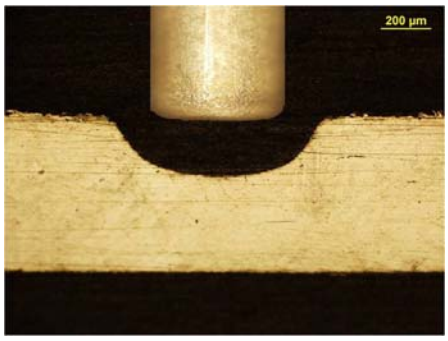

Figure 51

Cross section of a hole drilled in SS-316L at 50 KHz and 16 Vpp with electrode superimposed

Figure 51 shows a cross section of a hole drilled in 500 µm thick SS-316L with an image of electrode super imposed on it.

It was observed that the hole drilled was a replication of the tool profile. This showed that any profile could be machined with the appropriate design of tool.

6.3. DEBURRING RESULTS

µECM was successfully applied to deburr micro components. Figure 52 shows the component with burrs along the edges.

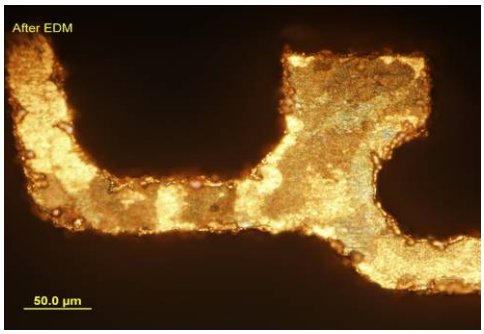

Figure 52

Micro electronic component with burrs along edges

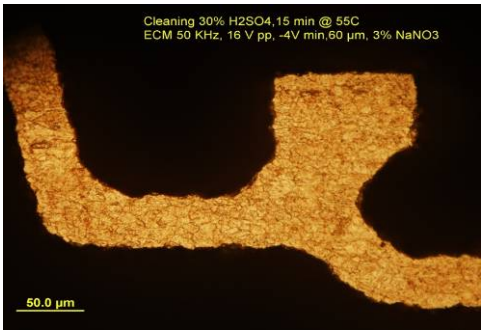

Figure 53

Component deburred with µECM at 50 KHz ,16 Vpp and ø500 µm tool

Table 12

Parameters for deburring calculated by model

Number of pulses	684000
Speed (μm/s)	137
Time (s)	14.62

The parameters for deburring as predicted by the model are tabulated in Table 12.

The experimental values which gave the best quality of deburred surface are tabulated in Table 13.

Table 13

Experimental parameters for deburring

Speed (μm/s)	125
Time (s)	16

The time predicted by the model and the experimental values are in close agreement. Figure 53 shows the workpiece after deburring it with electrochemical machining. It was observed that the burrs were removed enabling the workpiece to be used effectively for its end use.

7. CONCLUSIONS AND RECOMMENDATIONS

7.1. CONCLUSIONS

A novel μECM system was developed:

- Using high frequency pulses.
- A model was developed for material removal rate using pulsed current.
- The system was used to successfully form micro holes and for profile refinement.
- Experimental data on small drilled holes agreed with theoretical data within 10%.
- Micro burrs can be effectively removed by optimal μECM setup.

7.2. RECOMMENDATIONS

- Future work includes using ultrasonic vibrations and pulsed laser to enhance the process. It is assumed that the ultrasonic vibrations would enhance the rate at which the reaction products are flushed out of the machining zone resulting in a higher material removal rate. The pulsed laser would heat up the machining zone locally increasing the rate of anodic dissolution.
- The model for material removal rate can include the effect of pulse OFF duration and flow rate to accurately predict the material removal rate.

REFERENCES

ASM Metals Handbook Volume-8 (1973). Materials Park, OH : ASM International.

ASTM Standard A240. (2007). "Specification for Chromium and Chromium-Nickel Stainless Steel Plate, Sheet, and Strip for Pressure Vessels and for General Applications." ASTM International, West Conshohocken, PA. *http:// www.astm.org/*. Access date 04/01/2008.

ASTM Standard B196. (2007). "Specification for Copper-Beryllium Alloy Rod and Bar." ASTM International, West Conshohocken, PA. *http:// www.astm.org/*. Access date 04/01/2008.

Barber-Nichols Inc. (2008). "Picture of Turbine Machined by ECM" *http://www.barber-nichols.com/*. Access date 03/10/2008.

Bhattacharyya, B.; Malapati, M.; Munda, J.; and Sarkar, A. (2007). "Influence of tool vibration on machining performance in electrochemical micro-machining of copper." *Int'l Journal of Machine Tools and Manufacture* (v47, n2), pp335-342.

Bhattacharyya, B.; Malapati, M.; and Munda, J. (2005). "Experimental study on electrochemical micromachining." *Journal of Materials Processing Technology* (v169, n3), pp485-492.

Bhattacharyya, B. and Munda, J. (2003). "Experimental investigation on the influence of electrochemical machining parameters on machining rate and accuracy in micromachining domain." *Int'l Journal of Machine Tools and Manufacture* (v43, n13), pp1301-1310.

Center for Nontraditional Manufacturing Research, University of Nebraska Lincoln. (2007). "Theory of Electrochemical Machining" http*://www.unl.edu/nmrc/*. Access date 05/20/2007.

Da Silva Neto, J.; Da Silva, E.; and Da Silva, M. (2006). "Intervening variables in electrochemical machining." *Journal of Materials Processing Technology* (v179, n1-3), pp92-96.

Datta, M. (1993). "Anodic dissolution of metals at high rates." *IBM Journal of Research and Development* (v37, n2), pp207-226.

Datta, M. (1998). "Micro fabrication by electrochemical metal removal." *IBM Journal of Research and Development* (v42, n5), pp655-670.

Datta, M. and Landolt, D. (2000). "Fundamentals aspects and applications of electrochemical micro fabrication." *Electrochimica Acta* (v45, n15-16), pp2535-2558.

Datta, M. and Romankiw, L.T. (1989). " Application of chemical and electrochemical micromachining in the electronics industry." *Journal of the Electrochemical Society* (v136,n6), pp285-292.

Groover, M.P. (2000). *Fundamentals of Modern Manufacturing.* New York: John Wiley & Sons.

Hocheng, H.; Sun, Y.H.; Lin, S.C.; and Kao, P.S. (2003). "A material removal analysis of electrochemical machining using flat-end cathode." *Journal of Materials Processing Technology* (v140, n1-3), pp264-268.

Jack, H. (2001). "Theory of electrochemical machining" *http://www.eod.gvsu.edu/eod/manufact/manufact-281.html/.* Access date 05/25/2007.

Kim, B.; Ryu, S.; Choi, D.; and Chu, C. (2005). "Micro electrochemical milling." *Journal of Micromechanics and Microengineering* (v15, n1), pp124-129.

Kozak, J.; Rajurkar, K.P.; and Makkar, Y. (2004). "Selected problems of micro-electrochemical machining." *Journal of Materials Processing Technology* (v149, n1-3), pp426-431.

Kurita, T.; Chikamori, K.; Kubota, S. and Hattori, M. (2006). "A study of three-dimensional shape machining with an ECM system." *Int'l Journal of Machine Tools and Manufacture* (v46, n12-13), pp1311-1318.

Lenntech Water Treatment & Air Purification Holding B.V. (1998). "Properties of silicon" *http://www.lenntech.com/.* Access date 04/05/2008.

McGeough, J. (2005). "Theory of Electrochemical Machining" *http://www.electrochem.cwru.edu/ed/encycl/.* Access date 05/25/2007.

Mount, A.R.; Eley, K.L.; and Clifton, D. (2000). "Theoretical analysis of chronoamperometric transients in electrochemical machining and characterization of titanium 6/4 and inconel 718 alloys." *Journal of Applied Electrochemistry* (v30, n4), pp447-455.

Mukherjee, S.K.; Kumar, S.; Srivastava, P.K.; and Kumar, A.. (2007). "Effect of valency on material removal rate in electrochemical machining of aluminium." *Journal of Materials Processing Technology* (doi:10.1016).

Mukherjee, S.K.; Kumar, S. and Srivastava, P.K. (2005). " Effect of over voltage on material removal rate during electrochemical machining." *Tamkang Journal of Science and Engineering* (v8, n1), pp923-28.

Rajurkar, K.P.; Levy, G.; Malshe, A.; Sundaram, M.M.; McGeough, J.; Hu, X.; Resnick, R.; and DeSilva, A. (2006). "Micro and nano machining by electro-physical and chemical processes." *Annals of the CIRP* (v55, n2), pp643-666.

Rajurkar, K.P.; Zhu, D.; McGeough, J.A.; Kozak, J.; and DeSilva, A. (1999). "New developments in electro-chemical machining." *Annals of the CIRP* (v48, n2), pp567-579.

Stofesky, D.B. (2006). "Manufacturing with microECM." *Proc.* of 2006 ASME Intl.Conf. on Manufacturing Science and Engineering.

Viola, K.; Cagnon, L.; Schuster, R.; and Ertl, G. (2001). "Electrochemical machining of stainless steel microelements with ultrashort voltage pulses." *Applied Physics Letters* (v79, n11), pp1721-1723.

Yong, Li; Yunfei, Zheng; Guang, Yang and Liangqiang, Peng. (2003). "Localized electrochemical micromachining with gap control." *Sensors and Actuators* (v 108, n1-3), pp144-148.

APPENDIX A

DESIGN OF TOOL HOLDER AND ELECTROLYTE BATH

A view of the tool holder is given in Figure A-1. The various parts are numbered 1 through 6.

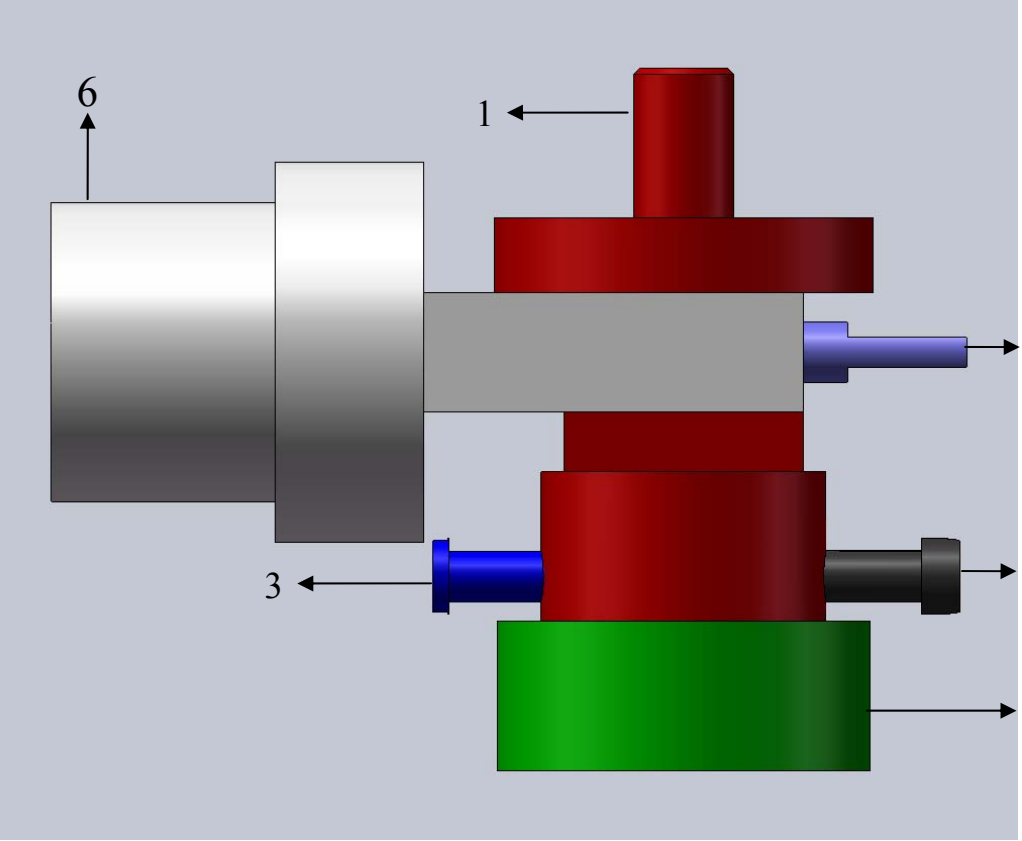

Figure A-1

Front view of tool holder

The tool holder consists of 5 parts. (1) is the main component of the tool holder. The hose from the pump through which the electrolyte flows is fastened to the holder at the narrow section at the top. The electrolyte then flows through the hollow section “A” in the middle as shown in Figure A-2.

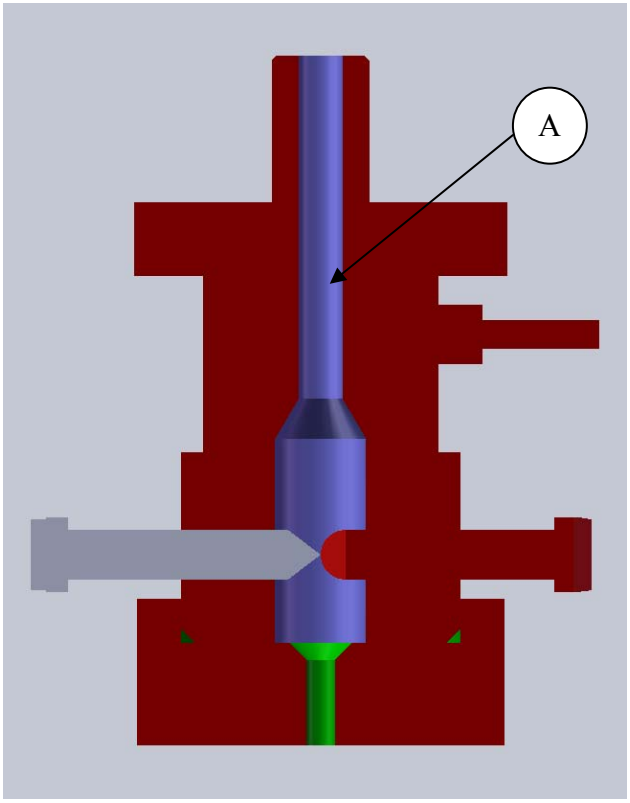

Figure A-2

Cross sectioned view of tool holder showing hollow portion

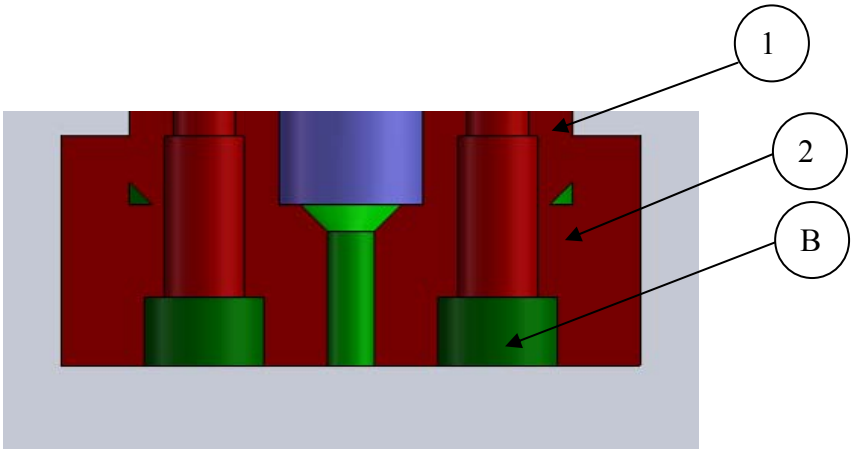

Figure A-3

Cross sectioned view of tool holder showing slots in component 2

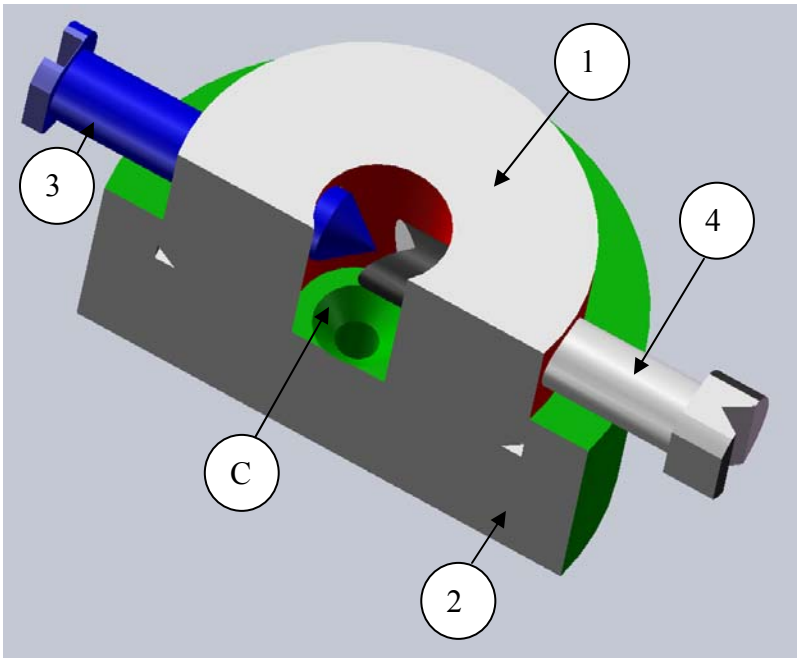

Figure A-4

Cross sectioned view of Solid model of tool holder showing component 2

The main purpose of (2) is to streamline the electrolyte flow. As shown in Figure A-3, (2) is fastened to (1) at the bottom. “B” is the slot for the fasteners. (3) and (4) are used to fasten the electrode and fit into the holes drilled on the sides of (1) a shown in Figure A-4. (3) is a screw whose end is machined into a conical section and similarly (4) is a screw on which a groove is machined at its end .The electrode is positioned in this groove and the screw with the conical section supports it from the other end, thereby ensuring that the electrode is rigidly clamped in position. The electrolyte enters the tool holder at the top and then flows around the electrode and is then streamlined by (2) by means of the conical section “C”, thus flowing uniformly all around the electrode and along its length. Three different pieces of “2” were made which can be interchanged.

The choice of the appropriate piece depends on the diameter of the electrode being used. Figure A-5 aids in the above discussion.

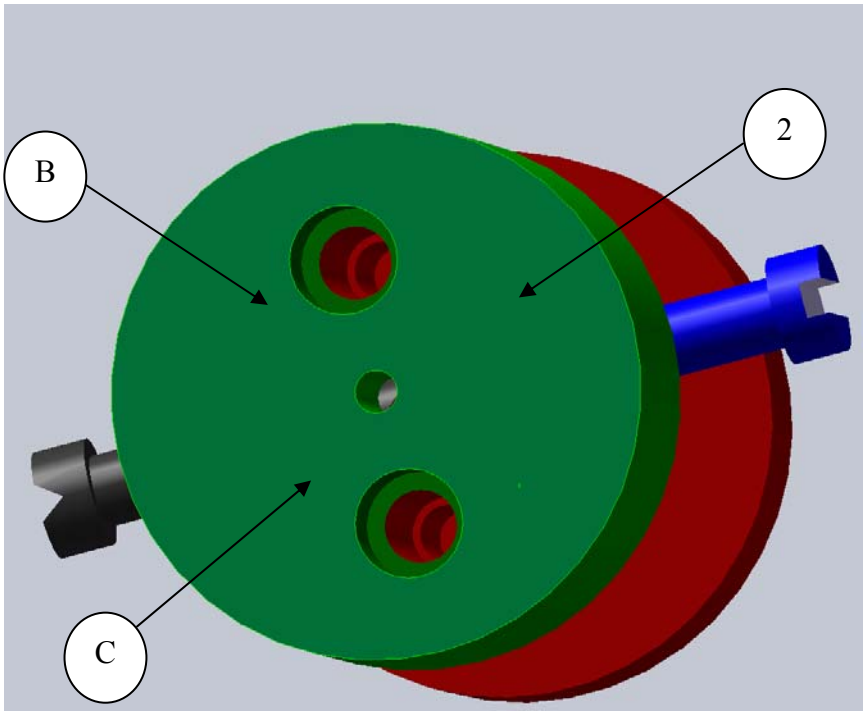

Figure A-5

Solid model with emphasis on modified component 2

The size of “C” varies in the three pieces. “2” is fastened to the body of tool holder “1” by means of step cap screws for better stability. “B” is the slot for the step cap screw. This assembly of (1), (2), (3), (4), (5) and the electrode is positioned on (6) by means of the groove on (1) and fastened by a screw to stay in place. The top surface of (5) is made flat and used for positioning purposes.

Selection of Material

The main criteria in the material selection are that it needs to be corrosion resistant and light weight at the same time. (1) and (2) were machined out of stainless steel because the electrolyte continuously flows through them and they need to withstand the corrosive effect of electrolyte. (4) was machined out of stainless steel because it supports the tool. (3) is used mainly for holding the tool in place and hence machined out of plastic to minimize the weight. (6) was machined out of stainless steel so that it is able to with stand the weight of the assembly. (6) is fastened to the slide controlled by a stepper motor.

For purposes of uniformity all the screws that were used were #6-32 or M3 including components (3) and (4).

The tool was held in position by the two screws whose ends were machined in an appropriate way. The electrode used was a cylindrical one. After much thought it was decided to make a small groove on the electrode, so that the screw positions itself in the groove avoiding further movement of the electrode. “D” is the groove that was machined on the electrode for clamping purposes as shown in Figure A-6.

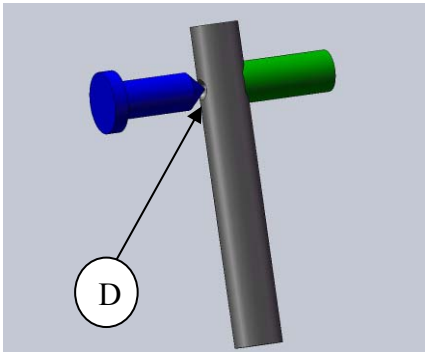

Figure A-6

Solid model of electrode showing the effect of groove

The groove was machined using Electric Discharge Machining (EDM). The machine used was Sodick K1C.The electrode used on the EDM was Ø0.8 mm copper tube. The electrode for ECM was clamped horizontally on the machine. The EDM electrode was brought into contact with the ECM electrode and the system zeroed down at that location. Once zeroed down at that location machining was done to a depth of 0.25 mm. A numbers of attempts with different parameters were made to find the optimal parameters. The optimal parameters that were found were,

ON Time: 12 OFF Time: 12

Voltage: 33 Current: 19

Figure A-7 shows a picture of the groove machined by EDM on a Ø1.3462 mm SS-316L electrode. The picture was taken on the Olympus STM6 Microscope.

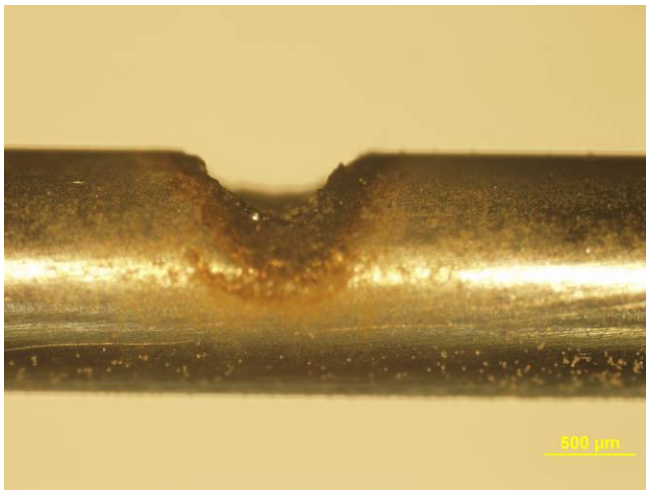

Figure A-7

Groove machined on SS-316L electrode

Figures A-8 and A-9 show the cross sectioned views of the electrolyte bath.

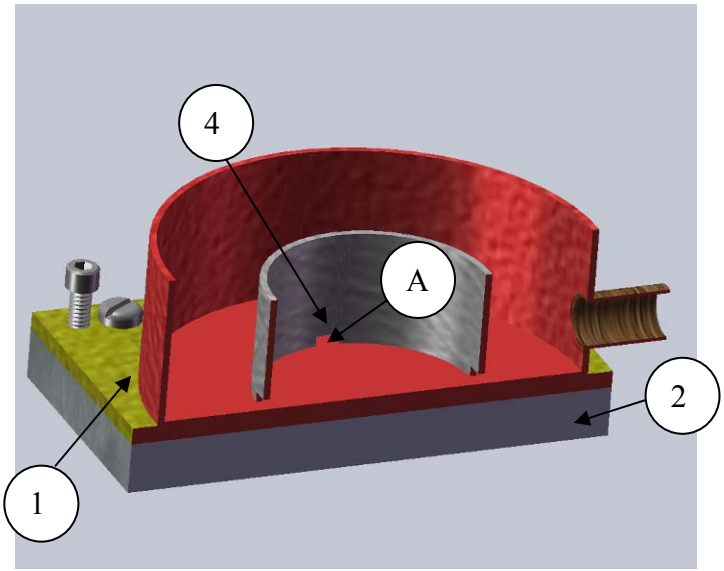

Figure A-8

Cross sectioned view of solid model of electrolyte bath showing grooves at bottom of A

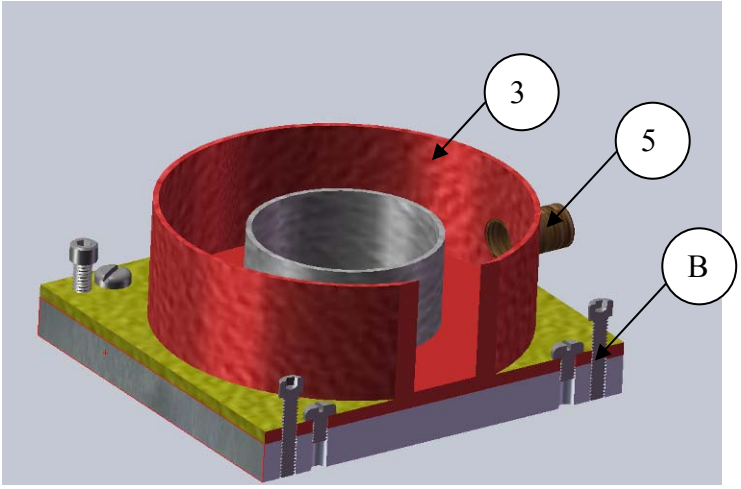

Figure A-9

Cross sectioned view of solid model of electrolyte bath showing screws

(1) and (2) are plates fastened together by means of screws with (1) on top of (2) as shown in Figure A-9. There is a separate set of screws “B” protruding out of base plate (2) as shown in Figure A-10 which were used for leveling purposes. (3) is a container that was glued onto the top surface of (1). This acted as the tank for collecting the electrolyte. (4) is a hollow component that was glued on to the inner surface of (3). Holes “A” were drilled on the sides of (4) as shown in Figure A-9 to allow the electrolyte to flow out otherwise the electrolyte would keep collecting there. The fixture holding the workpiece was mounted on (4). (5) is a hose running from the tank back to the pump which is for re-circulating the electrolyte in the system.

Selection of Material

(2) was machined out of aluminum whereas (1) wasmachined out of plastic. (3)

is a Compact Disc cake box made of plastic. A Compact Disc cake box was chosen because it is readily available and serves as a tank for holding the electrolyte. (4) is a plumbing pipe on which holes were drilled to enable flow of electrolyte.

The clamps were machined out of plastic and depending on the workpiece the appropriate one was chosen. The different clamps are shown in Figure A-10.

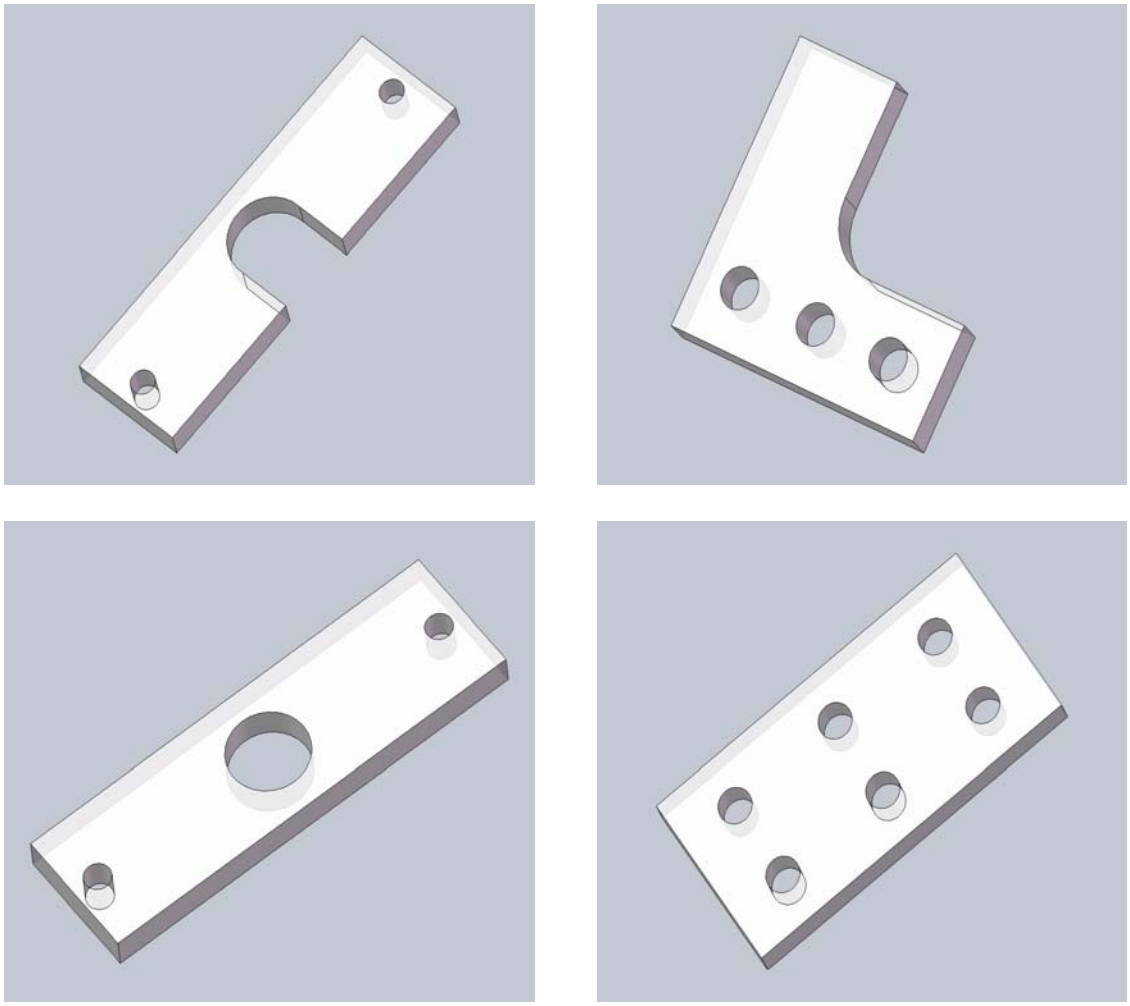

Figure A-10

Clamps

APPENDIX B

DETAILED DRAWINGS

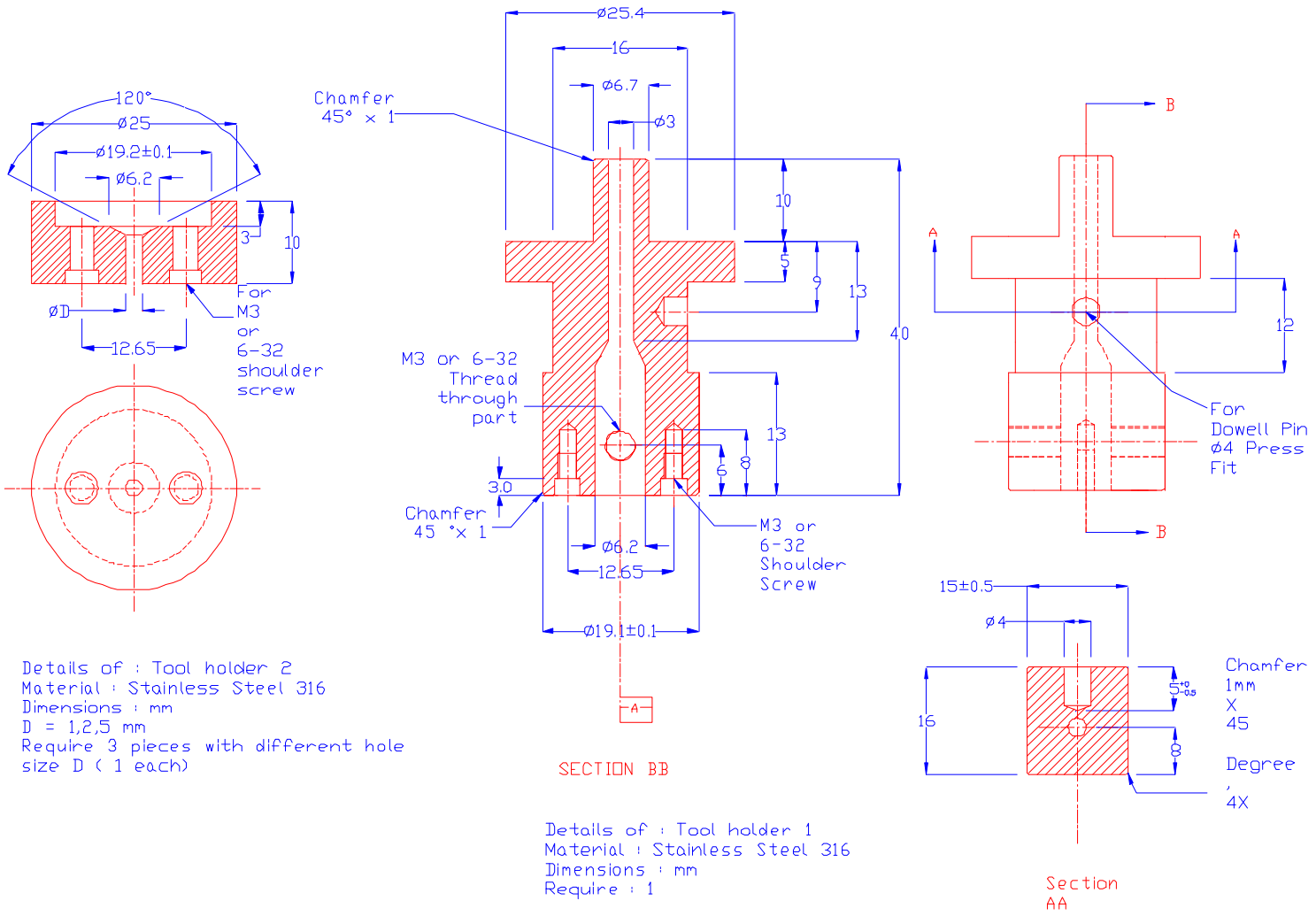
120°
ø25
ø19.2±0.1
ø6.2
3
10
øD
12.65
For
M3
or
6-32
shoulder
screw
Details of : Tool holder 2
Material : Stainless Steel 316
Dimensions : mm
D = 1,2,5 mm
Require 3 pieces with different hole
size D (1 each)
ø25.4
16
ø6.7
ø3
Chamfer
45° x 1
10
5
9
13
40
M3 or 6-32
Thread
through
part
13
6
8
3.0
Chamfer
45 °x 1
ø6.2
12.65
M3 or
6-32
Shoulder
Screw
ø19.1±0.1
A
SECTION BB
Details of : Tool holder 1
Material : Stainless Steel 316
Dimensions : mm
Require : 1
B
A
A
12
For
Dowell Pin
ø4 Press
Fit
B
15±0.5
ø4
16
Chamfer
1mm
X
45
Degree
,
4X
Section
AA

Figure B-1

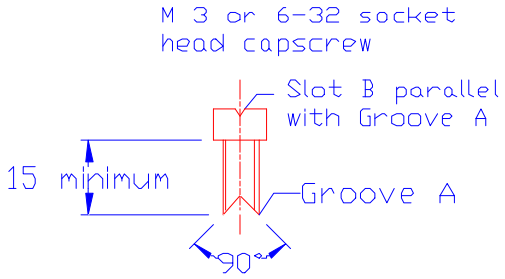

Details of : Tool holder 4
Material : Stainless steel 316
Dimensions : mm
Require : 2 pieces

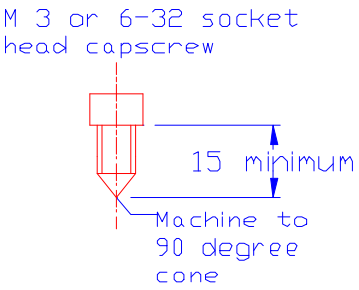

Details of : Tool holder3
Material : Plastic(nylon)
Dimensions : mm
Require : 2 pieces

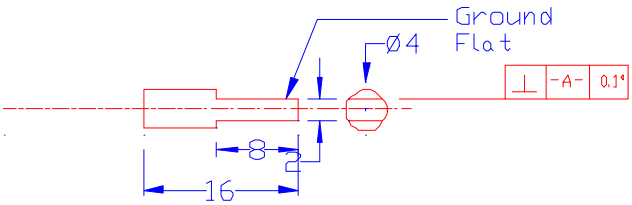

Details of : Tool holder5
Material : Stainless Steel 316
Dimensions : mm
Require : 1 piece

Figure B-2

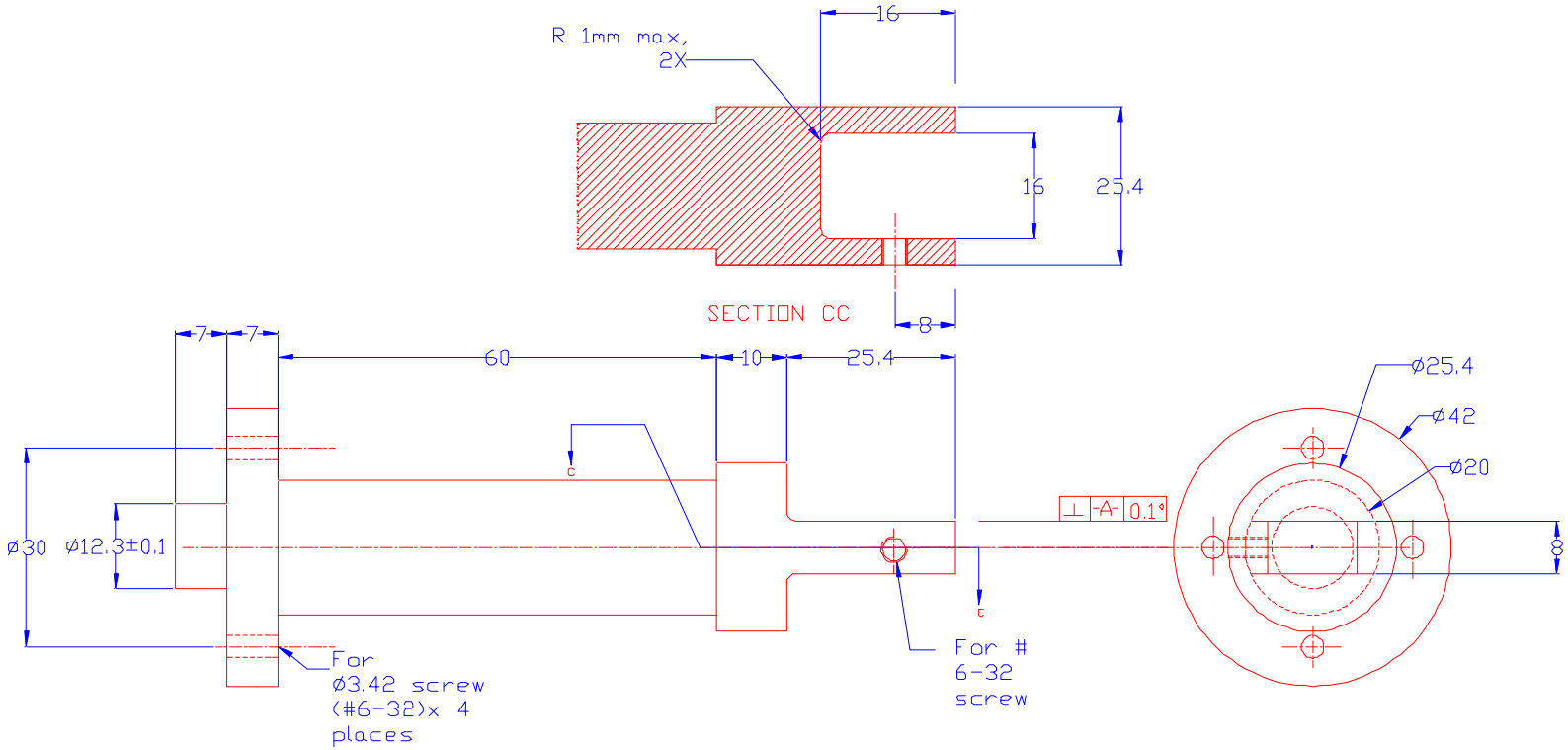

Details of : Tool holder 6
Material : Stainless Steel 316
Dimensions : mm
Require : 1 Piece

Figure B-3

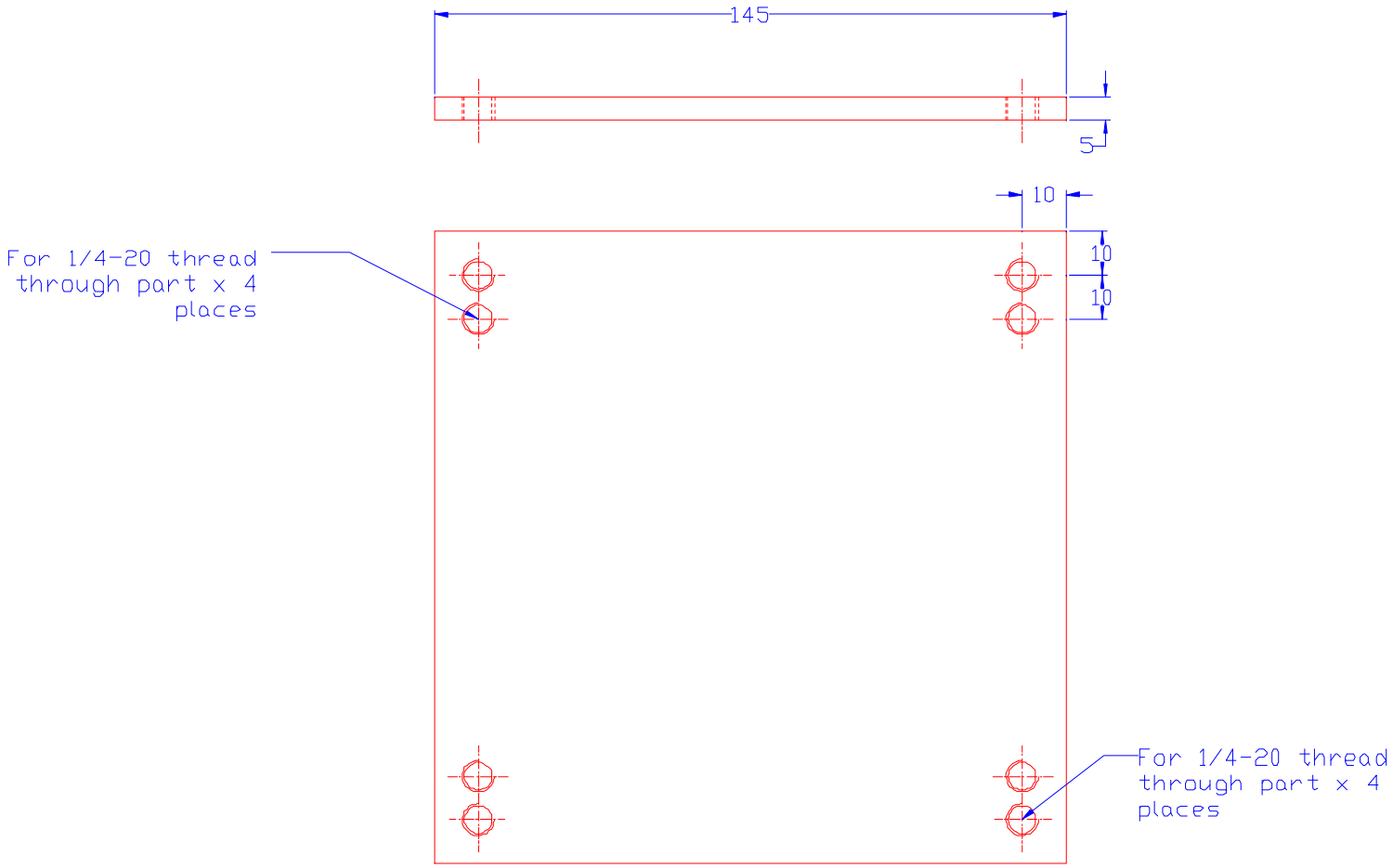

Details of : Electrolyte Bath 1
Material : Plastic(Nylon)
Dimensions : mm

Figure B-4

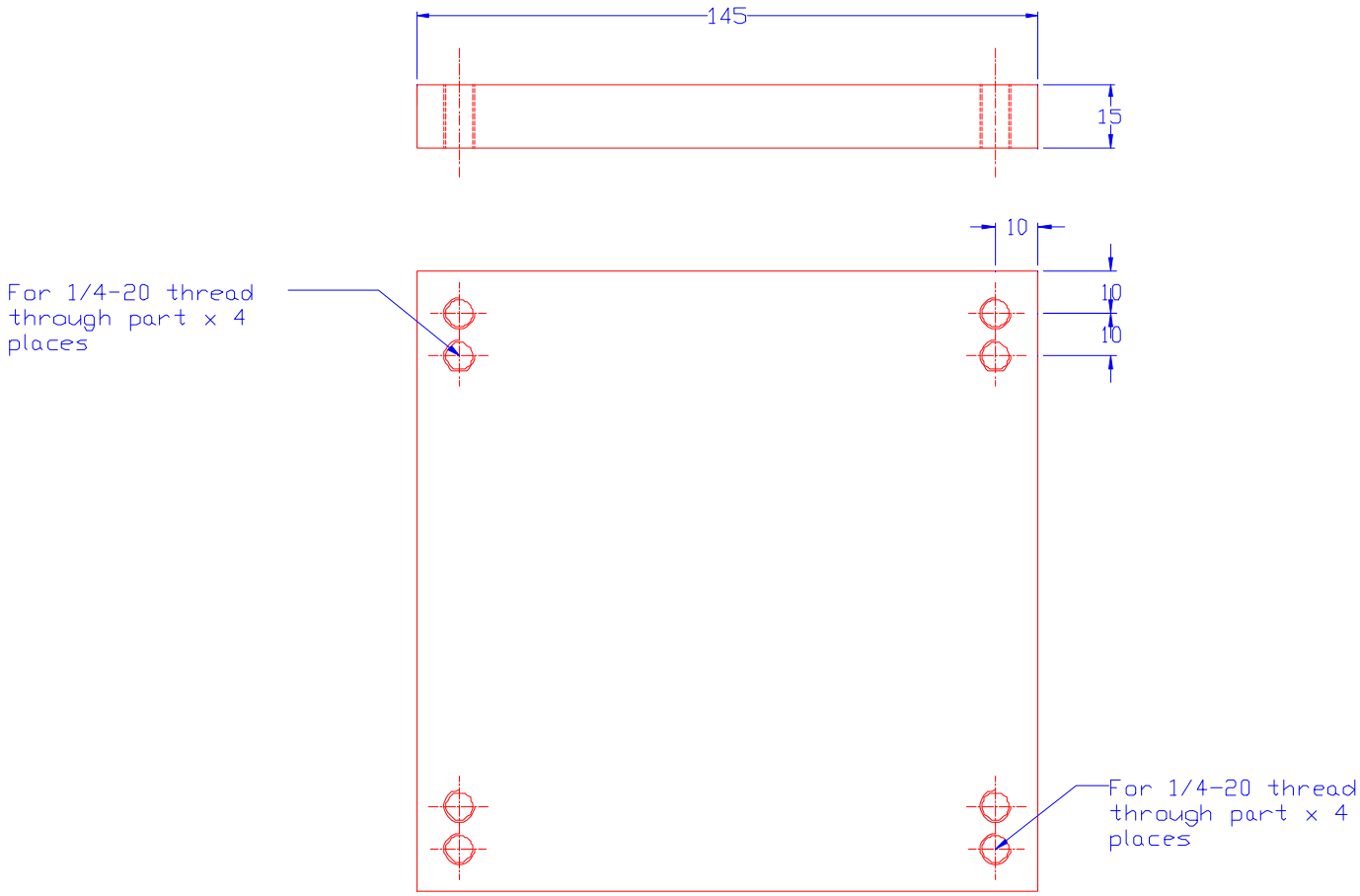

Details of : Electrolyte bath 2
Material : Stainless Steel
Dimensions : mm

Figure B-5

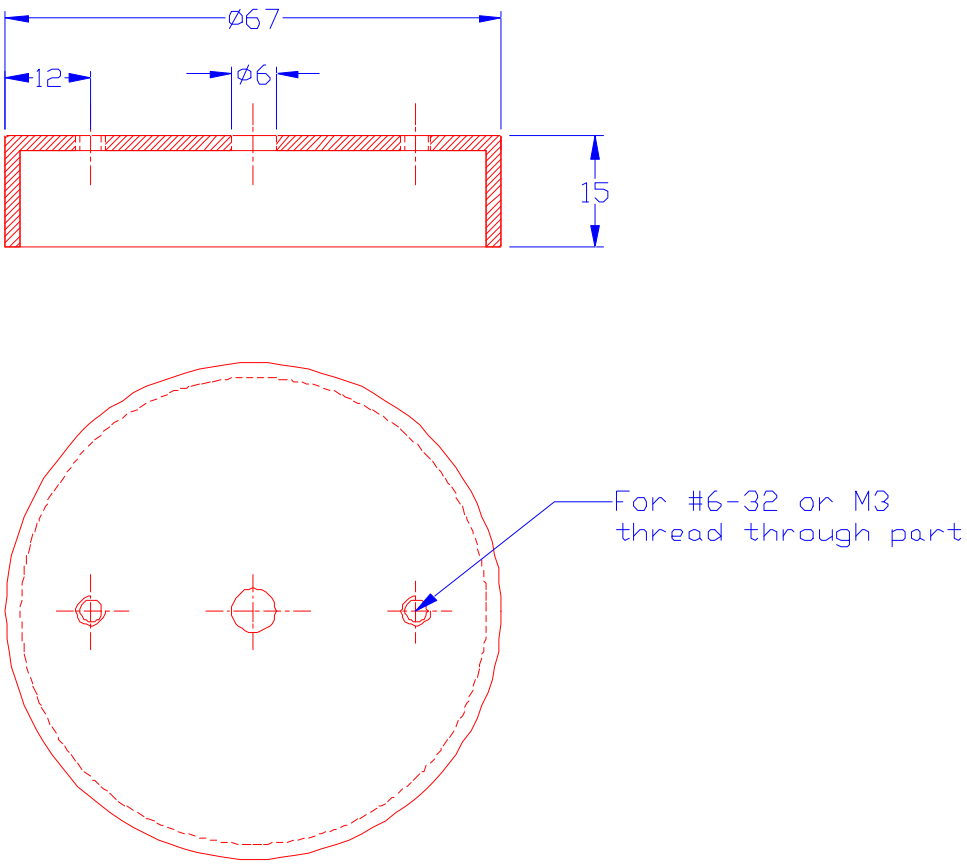
Ø67
12
Ø6
15
For #6-32 or M3
thread through part
Details of : Workpiece Fixture
Material : PVC
Dimensions : mm

Figure B-6

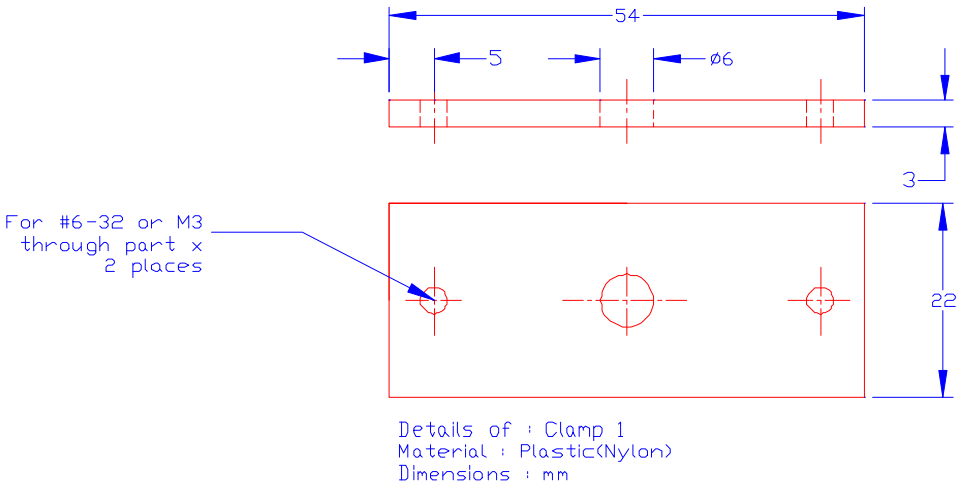
54
5
ø6
3
For #6-32 or M3
through part x
2 places
22
Details of : Clamp 1
Material : Plastic(Nylon)
Dimensions : mm

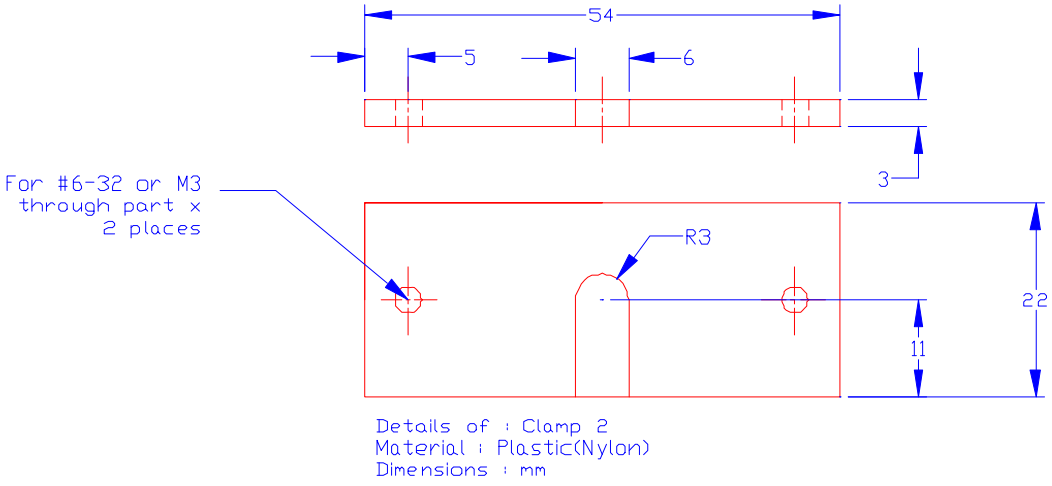
54
5
6
3
For #6-32 or M3
through part x
2 places
R3
22
11
Details of : Clamp 2
Material : Plastic(Nylon)
Dimensions : mm

Figure B-7

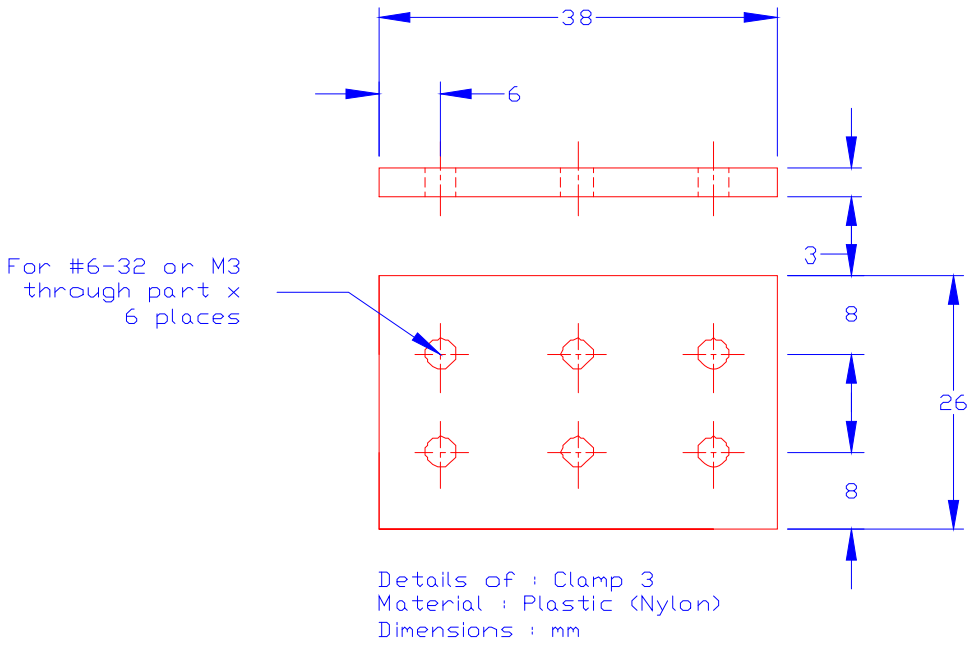
38
6
3
For #6-32 or M3
through part x
6 places
8
26
8
Details of : Clamp 3
Material : Plastic (Nylon)
Dimensions : mm

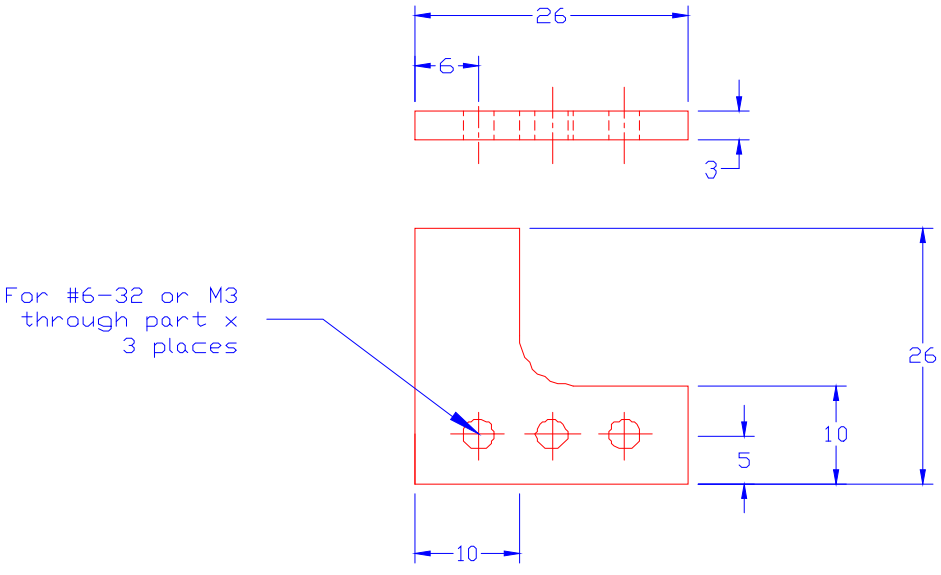
26
6
3
For #6-32 or M3
through part x
3 places
26
10
5
10
Details of : Clamp 4
Material : Plastic (Nylon)
Dimensions : mm

Figure B-8

APPENDIX C

COSMOS PROGRAMS

1. CA-173-40µm-2sec: This program drills hole to a depth of 40 µm in 100 µm thick copper sheet starting at a position 500 µm from the workpiece surface. It moves the tool at a higher speed till it reaches a height of 100 µm from worpiece surface and then slows down. The delay between the pulses is 2 seconds.

C S2M10,I2M180,LM0,S2M5,I2M1,P20,L36,LM0,S2M500,I2M-2000,R

Table C-1

Explanation of CA-173-40µm-2sec program

Code	Meaning
C	Clear memory
S2M10	Speed of motor 2 set to 10 steps per second
I2M180	Motor 2 moves 180 steps in the forward direction
LM0	Loop marker
S2M5	Speed of motor 2 set to 5 steps per second
I2M1	Motor 2 moves 1 step in forward direction
P20	Pause for 2 seconds
L36	Repeat the preceding commands until loop marker 36 times
LM0	Loop marker
S2M500	Speed of motor 2 set to 500 steps per seconds
I2M-2000	Motor 2 moves 2000 steps in the reverse direction
R	Execute program

2. CA-173-Through-2sec: This program drills through hole in 100 μm thick copper sheet starting at a position 500 μm from the workpiece surface. It moves the tool at a higher speed till it reaches a height of 100 μm from worpiece surface and then slows down. The delay between the pulses is 2 seconds.

C S2M10,I2M180,LM0,S2M5,I2M1,P20,L60,LM0,S2M500,I2M-2000,R

Table C-2

Explanation of CA-173-Through-2sec program

Code	Meaning
C	Clear memory
S2M10	Speed of motor 2 set to 10 steps per second
I2M180	Motor 2 moves 180 steps in the forward direction
LM0	Loop marker
S2M5	Speed of motor 2 set to 5 steps per second
I2M1	Motor 2 moves 1 step in forward direction
P20	Pause for 2 seconds
L60	Repeat the preceding commands until loop marker 60 times
LM0	Loop marker
S2M500	Speed of motor 2 set to 500 steps per seconds
I2M-2000	Motor 2 moves 2000 steps in the reverse direction
R	Execute program

3. SS-316L-100µm-2sec: This program drills through hole to a depth of 100 µm in 500 µm thick stainless steel sheet starting at a position 500 µm from the workpiece surface. It moves the tool at a higher speed till it reaches a height of 100 µm from worpiece surface and then slows down. The delay between the pulses is 2 seconds.

C S2M10,I2M180,LM0,S2M5,I2M1,P20,L60,LM0,S2M500,I2M-2000,R

Table C-3

Explanation of SS-316L-100µm-2sec program

Code	Meaning
C	Clear memory
S2M10	Speed of motor 2 set to 10 steps per second
I2M180	Motor 2 moves 180 steps in the forward direction
LM0	Loop marker
S2M5	Speed of motor 2 set to 5 steps per second
I2M1	Motor 2 moves 1 step in forward direction
P20	Pause for 2 seconds
L60	Repeat the preceding commands until loop marker 60 times
LM0	Loop marker
S2M500	Speed of motor 2 set to 500 steps per seconds
I2M-2000	Motor 2 moves 2000 steps in the reverse direction
R	Execute program

4. CA-173-Deburr: This program moves the tool across the surface of workpiece slowly to remove burrs. The tool is kept at a constant height as it moves along the surface.

C S2M180,I2M150,LM0,S2M25,I2M1,P3,L10,S1M70,I1M-2000,S2M500,I2M-160,R

Table C-4

Explanation of CA-173-Deburr program

Code	Meaning
C	Clear memory
S2M180	Speed of motor 2 set to 180 steps per second
I2M150	Motor 2 moves 150 steps in the forward direction
LM0	Loop marker
S2M25	Speed of motor 2 set to 25 steps per second
I2M1	Motor 2 moves 1 step in forward direction
P3	Pause for 0.3 seconds
L10	Repeat the preceding commands until loop marker 10 times
S1M125	Speed of motor 1 set to 125 steps per second
I1M-2000	Motor 1 moves 2000 steps in the reverse direction
S2M500	Speed of motor 2 set to 500 steps per second
I2M-160	Motor 2 moves 160 steps in the reverse direction
R	Execute program

VITA

Name:	Sriharsha Srinivas Sundarram
Address:	c/o Department of Mechanical Engineering, 3123 Texas A&M University, College Station, TX 77843.
Email Address:	sriharsha.ss@gmail.com
Education:	B.E., Manufacturing Engineering, Anna University, India, 2006 M.S., Mechanical Engineering, Texas A&M University, 2008